

INTENSIFIED DIMETHYL ETHER PRODUCTION FROM SYNTHESIS GAS
WITH CO₂

by

Nusret Furkan Öztürk

B.S., Chemical Engineering, Boğaziçi University, 2015

Submitted to the Institute for Graduate Studies in
Science and Engineering in partial fulfillment of
the requirements for the degree of
Master of Science

Graduate Program in Chemical Engineering
Boğaziçi University

2019

ACKNOWLEDGEMENTS

I would like to express my honest and deepest gratitude to my thesis supervisor, Prof. Ahmet Kerim Avcı. His expertise, priceless guidance, constant encouragement, loving attitude, understanding, patience, and healthy criticism added considerably to my experience. It would not have been possible for me to complete this study without his continual inspiration. You have been a tremendous mentor for me.

Besides my advisor, I would also like to thank Assoc. Prof. A. Kerem Uğuz and Assist. Prof. Gamze Gümüşlü Gür, my thesis committee for allocating their valuable time, their encouragement, insightful comments on my study. I would also like to express my appreciations to Assoc. Prof. Burak Alakent for his constant support and providing the help whenever it is needed, to Prof. A. Erhan Aksoylu and Prof. Uğur Akman for playing crucial roles on the stage shaping me who I am today.

Special mention to Ege Belit Munis, a gorgeous woman who knows me and understands me better than anyone else, perhaps except her cat, she understands even better. I wish to express my sincere thanks to Ahmet Hallaçeli, for a close friendship we have developed together in a short time, hospitality in his hometown Adana and endless joyful ‘yeee’ memories. The best is yet to come. I cannot think of a life without my childhood friends; Halil Güçlü, Melih Bayır, Furkan Oğuz, Numan Özkara, Osman Erken, Semih Gülen, Suat Çelebi, Yusuf Topçu, Murat Kaygusuz, Onur Yıldırım, and Taha Gocuk. Thank you for never ending black humor and pushing me to complete my masters in a way you do not recognize.

I sincerely admire the contribution of all my lab friends in KB-404; Sinan Koç, Mert Özden, Semih Altınsoy, Özge Selçuk, and Uğurcan Tozar for times we share meals and lots of laughter. However, I am profoundly thankful to Selin Baç Bilgi for extended discussions, valuable suggestions, being an excellent superior and cheerful memories both in and out of the university. You are like Hera in today’s world, ruling over KB-404 instead of Mount Olympus.

I want to thank Ece ıđdem Mutlu, Mge Kasım, Sercan Altundemir, Cořkun Bilgi, Cihat ztepe, Dilara Greke, İlke Kaykanat, Serhat Erřahin, Aslı řahin, Aysun Urhan, ađla Odabařı, Elif Can, Elif Gentrk, Begm Yađcı, Elif Esvap and Talha Ayar for all kinds of experiences and memories.

I extend my thanks to the fellow staff in the chemical engineering department Yakup Bal, Belgin Balkan, Murat Dzgnođlu and řkr Ordu.

I am immensely indebted to my father; every time I fail you ask *me why do we fall* and continue to show what a magnificent human being you are in every situation. Thank you, my mother, for endless support and constant inspiration for my journey in this life. Heartfelt thanks go to my lovely sisters; life would have been utterly meaningless without you two.

Last but certainly not least, I feel a profound sense of gratitude to my fascinating little darling Saime, who lightens the path I walk with her boundless cheer and love. You are like springtime come alive. Thank you for everything.

Finally, financial support provided by TBİTAK BİDEB 2210-A and TBİTAK 118M518 are acknowledged.

ABSTRACT

INTENSIFIED DIMETHYL ETHER PRODUCTION FROM SYNTHESIS GAS WITH CO₂

Catalytic conversion of syngas to dimethyl ether (DME) is modeled in a microchannel reactor comprised of horizontal groups of rectangular shaped cooling and catalyst washcoated reaction channels involving counter-current flows of air and syngas, respectively. The steady-state model, deviating from the literature-based experimental data in the range of 3–14%, involves two-dimensional conservation of momentum, heat and species mass together with inter-channel heat exchange and reactive transport within porous catalyst layer composed of equivalent mass of uniformly mixed Cu-ZnO/Al₂O₃ and γ -Al₂O₃ catalysts. For the first time in the literature, the benefits of functional and volumetric intensification on the precise regulation of the interplay between exothermic equilibrium synthesis and dehydration reactions are demonstrated. Feeding syngas to the air-cooled microchannel reactor at 508 K, 50 bar, H₂/CO=2.5 and H₂/CO₂=10 elevates the inlet temperature by only 9 K which is significantly below 40 K of identically operated packed-bed tubular reactors. Increasing syngas feed temperature from 493 to 508 K elevates CO conversion from 33 to 45%, which eventually shifts DME yield from 2 to 3.6%. Similar qualitative trends are observed upon pressurizing syngas as well as feeding it at higher flow rates under CO-rich and CO₂-lean conditions, all of which fundamentally promote CO hydrogenation, the primary contributor of the exothermic temperature rise that subsequently improves reactor performance under the control of intensified cooling. Even though they promote better regulation of hot-spot formation, the impacts of using thicker walls between the channels and thermally conductive reactor materials remain negligible.

ÖZET

CO₂ İÇERİKLİ SENTEZ GAZINDAN YOĞUNLAŞTIRILMIŞ DİMETİL ETER ÜRETİMİ

Sentez gazının dimetil etere (DME) katalitik dönüşümü, dikdörtgen kesitli soğutma ve katalizörün iç duvarlarına ince bir tabaka şeklinde kaplı olarak bulunduğu reaksiyon kanallarını barındıran, hava ile sentez gazının zıt yönlü olarak beslendiği bir mikro kanal reaktörde modellenmiştir. Literatüre dayalı deneysel verilerden %3-14 aralığında sapan bu model; yatışkın halde iki boyutta momentum, ısı ve kütle değişimleri, kanallar arası ısı transferi ve eşit ağırlıklarda karıştırılmış olarak kanal iç duvarına ince, gözenekli bir tabaka halinde kaplı bulunan Cu-ZnO/Al₂O₃ ve γ -Al₂O₃ katalizörleri üzerinde gerçekleşen reaksiyonları içermektedir. Literatürde ilk defa, ekzotermik denge sentezi ile dehidrasyon reaksiyonları arasındaki etkileşimin fonksiyonel ve hacimsel yoğunlaştırma ile hassas bir biçimde kontrol edilebildiği gösterilmiştir. Sentez gazını, hava soğutmalı mikro kanal reaktöre 508 K, 50 bar, H₂/CO=2.5 ve H₂/CO₂=10 oranlarında beslemek reaktör içi sıcaklığı sadece 9 K artırmaktadır. Benzer koşullarda aynı sıcaklık artışı dolgu yataklı tüp tipi reaktörlerde 40 K'dir. Sentez gazı besleme sıcaklığının 493 K'den 508 K'e yükseltilmesi CO dönüşümünü %33'ten %45'e, bu artış DME eldesini %2'den %3.6'ya artırmaktadır. Benzer artış eğilimleri sentez gazının basınçlandırılması, giriş hızının artırılması ve yüksek CO, düşük CO₂ içerikli besleme koşullarında da gözlemlenmiştir. Bu parametrelerin tümü, sıcaklık artışının ana sebebi olan CO hidrojenasyonunu teşvik etmekte olup bu durum yoğunlaştırılmış soğutma kontrolündeki reaktörün performansını artırmaktadır. Sıcak-nokta oluşumunu engellemesine karşın, kanallar arası duvarın kalınlığındaki artışın ve reaktörün ısı iletim katsayısı daha yüksek materyaller ile imal edilmesinin etkileri göz ardı edilebilir olarak hesaplanmıştır.

TABLE OF CONTENTS

ACKNOWLEDGEMENTS	iii
ABSTRACT	v
ÖZET	vi
LIST OF FIGURES	viii
LIST OF TABLES	x
LIST OF SYMBOLS	xi
LIST OF ACRONYMS/ABBREVIATIONS	xiii
1. INTRODUCTION	1
2. LITERATURE SURVEY	7
2.1. Dimethyl Ether Production	7
2.1.1. Indirect DME Synthesis	8
2.1.2. Direct DME Synthesis and Intensification	11
3. MATHEMATICAL MODELING	14
3.1. Details of the Microchannel Reactor	14
3.2. Reaction Network and the Kinetic Model	15
3.3. Reactor Operation, Overview of the Parametric Study and Numerical Solution	19
4. RESULTS AND DISCUSSION	24
4.1. Validation of the Reactor Model	24
4.2. Effect of Syngas Feed Temperature	25
4.3. Effect of Syngas Feed Pressure	29
4.4. Effect of Molar Inlet H ₂ /CO ratio	31
4.5. Effect of molar inlet H ₂ /CO ₂ ratio	33
4.6. Effects of Inlet Flow Rate	35
4.7. Effects of Wall Thickness and Material	37
4.8. Effects of Flow Partitioning	40
5. CONCLUSION	42
5.1. Recommendations	43
REFERENCES	44

LIST OF FIGURES

Figure 1.1.	Energy sources of the world [3].	2
Figure 1.2.	Hot-spot formations inside tubular packed bed reactors (adopted from [14, 15], as solid line and dashed line, respectively).	5
Figure 2.1.	DME production diagram [4].	8
Figure 2.2.	DME sytnhesis from methanol, second part of indirect route [4].	9
Figure 2.3.	Indirect DME sytnhesis from syngas [4].	10
Figure 3.1.	Simplified (not to scale) illustrations of the intensified, microchannel DME synthesis reactor (left) and the unit cell (adopted from [64])	14
Figure 4.1.	Comparison of the experimental and predicted syngas conversions. Experimental data is taken from [49].	24
Figure 4.2.	Evolution of (a) temperature, (b) CO conversion, (c) rates of methanol synthesis reactions, yields of (d) steam and (e) methanol, and (f) rate of methanol dehydration along the reaction channel at different syngas feed temperatures.	26
Figure 4.3.	Evolution of (a) temperature, (b) CO conversion, (c) rates of methanol synthesis reactions, yields of (d) steam and (e) methanol, and (f) rate of methanol dehydration along the reaction channel at different syngas feed pressures.	29

Figure 4.4.	Evolution of (a) temperature, (b) CO conversion, (c) rates of methanol synthesis reactions, yields of (d) steam and (e) methanol, and (f) rate of methanol dehydration along the reaction channel at different molar inlet H_2/CO ratios	32
Figure 4.5.	Evolution of (a) temperature, (b) CO conversion, (c) rates of methanol synthesis reactions, yields of (d) steam and (e) methanol, and (f) rate of methanol dehydration along the reaction channel at different molar inlet H_2/CO_2 ratios	34
Figure 4.6.	Evolution of (a) temperature, (b) CO conversion, (c) rates of methanol synthesis reactions, yields of (d) steam and (e) methanol, and (f) rate of methanol dehydration along the reaction channel at different molar inlet velocities.	36
Figure 4.7.	Evolution of (a) temperature, (b) CO conversion, (c) rates of methanol synthesis reactions, yields of (d) steam and (e) methanol, and (f) rate of methanol dehydration along the reaction channel at different solid wall thickness values.	38
Figure 4.8.	Evolution of (a) temperature, (b) CO conversion, (c) rates of methanol synthesis reactions, yields of (d) steam and (e) methanol, and (f) rate of methanol dehydration along the reaction channel at different wall materials.	39
Figure 4.9.	Evolution of (a) temperature, (b) CO conversion, (c) rates of methanol synthesis reactions, yields of (d) steam and (e) methanol, and (f) rate of methanol dehydration along the reaction channel at different flow partitionings.	40

LIST OF TABLES

Table 1.1.	Physical properties of DME. (adapted from [4])	3
Table 3.1.	Temperature dependence of the parameters used in the kinetic model (adapted from Hu <i>et al.</i> [15])	16
Table 3.2.	The van der Waals coefficients used for evaluation of Equation 3.4 (adapted from [67])	17
Table 3.3.	Constants needed for the estimation of Gibbs free energy of formation of the species (adapted from [68])	18
Table 3.4.	Model equations used to simulate DME synthesis within the unit cell (Figure 3.1)(adapted from [69])(FP: fluid phases in reaction and cooling channels, CWP: catalytic washcoat phase in reaction channel, SW: solid wall between the channels)	20
Table 4.1.	DME yield obtained as functions of operating conditions	28

LIST OF SYMBOLS

C_2	Inertial resistance coefficient of the washcoat (m^{-1})
cat	Catalyst
$c_{p,m}$	Heat capacity of gas mixture ($\text{J kg}^{-1} \text{K}^{-1}$)
$D_{eff,i,m}$	Effective diffusivity of species i in the mixture, ($\text{m}^2 \text{s}^{-1}$)
$D_{i,m}$	Diffusivity of species i in the mixture, ($\text{m}^2 \text{s}^{-1}$)
$d_{particle}$	Particle diameter (m)
eff	Effective
f_i	Fugacity of species i in the mixture (bar)
$f_{pure,i}$	Fugacity of pure species i (bar)
\vec{F}	Momentum source/sink term ($\text{kg m}^{-2} \text{s}^{-2}$)
$G_{f,i}$	Gibbs free energy of formation of species i (kJ mol^{-1})
$H_{f,i}$	Enthalpy of formation of species i (kJ mol^{-1})
\mathbf{I}	3x3 identity matrix
i	Species indices
\vec{J}_i	Diffusive mass flux of species i ($\text{kg m}^{-2} \text{s}^{-1}$)
$K_{D,rxn}$	Reaction equilibrium constant (MS1 and MS2; bar^{-2} , MD; -)
K_i	Adsorption/desorption equilibrium constant for species i (bar^{-1})
$k_{eff,m}$	Effective thermal conductivity of gas mixture in the washcoat layer ($\text{W m}^{-1} \text{K}^{-1}$)
k_{rxn}	Reaction rate constant (MS1; $\text{kmol m}^{-3} \text{s}^{-1} \text{bar}^{-3}$, MS2; $\text{kmol m}^{-3} \text{s}^{-1} \text{bar}^{-4}$, MD; $\text{kmol m}^{-3} \text{s}^{-1} \text{bar}^{-1}$)
k_m	Thermal conductivity of gas mixture ($\text{W m}^{-1} \text{K}^{-1}$)
k_w	Thermal conductivity of the solid wall ($\text{W m}^{-1} \text{K}^{-1}$)
L	Microchannel length (m)
m	Mixture
M_i	Molecular weight of species i (kg mol^{-1})
n_i	Number of moles of species i (mol)
Nu	Nusselt number

P	Total pressure (bar)
p	Particle
r_{rxn}	rate of reaction (MS1, MS2, MD; kmol m ⁻³ s ⁻¹)
R	Gas constant (=8.314 J mol ⁻¹ K ⁻¹)
R_i	Consumption/generation rate of species i (kmol m ⁻³ s ⁻¹)
Re	Reynolds number
rxn	Reaction
$S_{f,i}$	Entropy of formation of species i (kJ mol ⁻¹ K ⁻¹)
Sh	Sherwood number
T	Temperature (K)
\vec{v}	Velocity vector (m s ⁻²)
w	Solid wall phase
x, y, z	Cartesian coordinates
y_i	Mole fraction of species i
Y_i	Mass fraction of species i
α	Permeability of the washcoat (m ²)
ΔG_{rxn}	Gibbs free energy of reaction (MS1, MS2, MD; kJ mol ⁻¹)
ΔH°	Standard enthalpy of reaction (kJ mol ⁻¹)
ΔH_{rxn}	Enthalpy of reaction (MS1, MS2, MD; kJ mol ⁻¹)
ϵ_{cat}	Porosity of the washcoat layer
μ_i	Viscosity of species i, (kg m ⁻¹ s ⁻¹)
μ_m	Average gas mixture viscosity, (kg m ⁻¹ s ⁻¹)
ρ_m	Density of gas mixture, (kg m ⁻³)

LIST OF ACRONYMS/ABBREVIATIONS

2D	Two dimensional
CH ₃ OH	Methanol
CH ₃ OCH ₃	Dimethyl ether
CH ₄	Methane
CO	Carbon monoxide
CO ₂	Carbon dioxide
CZA	Copper-Zinc oxide-Alumina
DME	Dimethyl ether
H ₂	Hydrogen
H ₂ O	Water/steam
HZSM-5	Zeolite socony mobil no. 5
LPG	Liquified petroleum gas
MS1	Methanol synthesis from carbon monoxide
MS2	Methanol synthesis from carbon dioxide
MD	Methanol dehydration
Mboe/d	Million barrels of oil equivalent per day
MW	Molecular weight
N ₂	Nitrogen
NO _x	Nitrogen oxides
RWGS	Reversed water-gas shift
STY	Space time yield
WGS	Water-gas shift

1. INTRODUCTION

Since the 1900s energy consumption has increased exponentially as the world population has increased almost five times from 1.6 billion to 7.3 billion [1]. Fossil fuels are still the primary energy sources for meeting the energy demand around the world, and among them crude oil has the highest share. Some incentives; such as continuously increasing fossil fuel consumption, environmental problems such as greenhouse gas emissions caused by burning fossil fuels and fluctuating price tags encourage researchers to find reliable and sustainable energy supplies. Besides, the results of possible inadequate oil availability is expected to be severe since the world economy depends strongly on oil [2]. In that manner, shifting to renewable energy has the potential to overcome the adverse effects of conventional energy sources. In the context of such a strategy, greenhouse gas emissions can be diminished, thereby extreme weather and climate impacts can be prevented, and cost-efficient, reliable and timely energy delivery can be sustained [3].

Renewable energy can be created from the sun either directly; by means of thermal, photo-chemical, photo-electric, or indirectly; via wind and hydro-power. Tidal and geothermal energy and photosynthetic energy stored in biomass are the other renewable energy sources. Since these sources are continuously replenished by the nature, they have capacity to provide over 3000 times the current global energy demand as can be seen from Figure 1.1 [3].

Biomass is the term used for all organic material deriving from plants, trees and crops. Biomass energy or bioenergy is the transformation of these organic materials into valuable forms of energy such as electricity, heat and liquid fuels, i.e. biofuels. Even though biomass energy is renewable and sustainable, it has mutual characteristics with fossil fuels. Biomass can either be burned directly to obtain energy or can be used as a feedstock to be converted to various liquids. Similar to their fossil counterparts, it is possible to store and transport biofuels. As a result, developing biorefinery and biotransformation technology to produce clean energy fuels from biomass feedstock

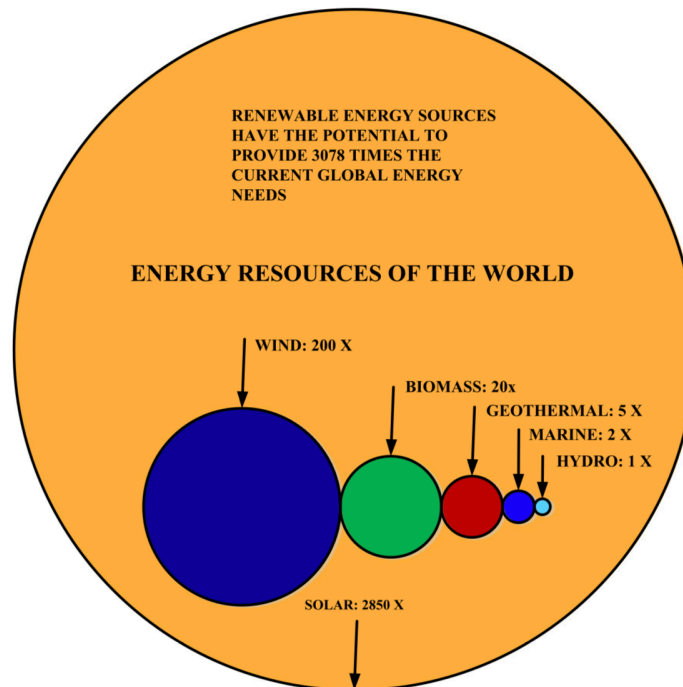


Figure 1.1. Energy sources of the world [3].

gains importance. Conversion of biomass feedstock into bioenergy can be achieved by thermo-chemical and bio-chemical processes including combustion, gasification and pyrolysis [3].

Biomass is expected to have a crucial role in the future of energy. Consumption of biofuels, which are mainly used in road transport, is predicted to reach 4.5 million barrels of oil equivalent per day (mboe/d) in 2035 from 1.3 mboe/d in 2010. Biomass plant capacity increased from 66 GW in 2010 to 72 GW in 2011, and forecasted production is 270 GW by 2030, globally [3]. Among biofuels, dimethyl ether (DME) is considered as a strong candidate for replacing their conventional counterparts in the near future due to its attractive properties such as easy transportation and handling, and pollutant (i.e. CO, NO_x) free combustion characteristics [4].

DME is a volatile compound, and it creates a liquid phase when it is pressurized at around 5 bar which allows DME to be handled and stored as liquid. DME has similar features with butane and propane, and it burns with a visible blue flame, which makes DME an alternative to LPG for heating and home cooking. DME is considered

as a clean fuel due to several reasons. Its storage and handling are safe since it does not form explosive peroxides, unlike other homologous ethers. DME only consists of C-H and C-O bond, and it does not contain any C-C bond. This property results in less carbon monoxide and unburned hydrocarbon emissions compared to those of natural gas when they are both burned. Having high cetane number (55-60 for DME, 40-50 for diesel [5]) makes DME an excellent transportation fuel alternative with no emission of toxic gases and particulate matters. DME can be utilized with existing storage and transportation infrastructures because of its vapor pressure similar to that of LPG. DME can also be used as a pesticide, and polishing and anti-rust agent. It can be used for producing alkyl-aromatics which are vital compounds used hydrogen production used in fuel cells [4]. The value of DME market is projected to be \$9.5 billion by 2020, with an average yearly growth of 19% between 2015 and 2020 [6].

Table 1.1. Physical properties of DME. (adapted from [4])

Molecular formula	C_2H_6O
Molar mass	46.07 g mol^{-1}
Appearance	Colorless gas
Odor	Typical
Density	1.97 g cm^{-3}
Melting point	$-141 \text{ }^\circ\text{C}$, 132 K
Boiling point	$-24 \text{ }^\circ\text{C}$, 249 K
Solubility in water	71 g dm^{-3} at (20 $^\circ\text{C}$)
Vapor pressure	$>100 \text{ kPa}$

The feedstock for DME production is synthesis gas (syngas), a mixture of carbon oxides (mostly CO) and H_2 , whose composition depends on the hydrocarbon type (natural gas, coal or biomass) and the production route, i.e. either catalytic reforming or gasification with steam, CO_2 or oxygen [7]. DME can be produced in two different ways. Conventional DME production is carried out by the indirect route that involves two sequential catalytic packed-bed reactors. The first reactor includes a synthesis catalyst, typically Cu-ZnO/ Al_2O_3 or HZSM-5 to drive syngas-to-methanol conver-

sion, whereas a solid acid catalyst such as $\gamma\text{-Al}_2\text{O}_3$ is used to dehydrate methanol to DME [4, 8]. This production method requires high pressures (60–150 bar) to increase syngas conversions, due to thermodynamic limitations of the methanol synthesis reaction [9]. In the direct synthesis route, however, reactions run within the same reactor at temperature and pressure ranges of 493–573 K and 10–50 bar, respectively on a bed composed of either a physical mixture of the synthesis and dehydration catalysts or of a single, hybrid catalyst in which active phases for synthesis and dehydration reactions exist on the same support [4, 8]. Indirect process is utilized to produce DME in companies such as Lurgi, MGC, Toyo and Udhe, and direct production process technology belongs to companies such as Air Products, Haldor Topsoe, JFE Holdings, Korea Gas Corporation and NKK [10]. Commercialization of direct route dates back to 2005, when JFE Holdings successfully scaled-up its pilot DME production plant to achieve 100 ton DME per day at Hokkaido, Japan. Besides JFE Holdings no other company has achieved industrial scale production. The rest are on the track of commercialization but currently they are at pilot-plant production level [11].

Compared with the conventional production method, the direct route allows higher CO conversion and simpler reactor designs. Direct approach also favors immediate consumption of methanol upon its formation, and therefore thermodynamically promotes methanol synthesis from both CO and CO₂. This functional benefit eliminates the dependence of the total operating expense on the cost of making methanol [12, 13]. Moreover, reduction in the capital and operating expenses associated with the use of a single reactor unit is an additional advantage of the direct route. Nevertheless, more complex separation process is required to obtain high purity DME due to unreacted syngas and produced CO₂ presence in the products [4].

Temperature regulation becomes crucial when DME is produced by the direct route due to highly exothermic reactions involved in the reaction network. Examples of temperature profiles and hot-spot formations of ~ 40 K are given in Figure 1.2. The difference between hot-spot locations arises from the cooling type selection; as Vakili [14] (solid line) balanced heat release with series of endothermic reactions whereas Hu *et al.* [15] (dashed line) cooled the reactor with counter-currently fed steam. Hot-

spot formation inside a reactor may cause rapid catalyst deactivation, undesirably high outlet temperatures or even run-away. Moreover, temperature is the vital parameter for keeping the balance between the kinetics and thermodynamics of the exothermic equilibrium-limited methanol synthesis and dehydration reactions. In this respect,

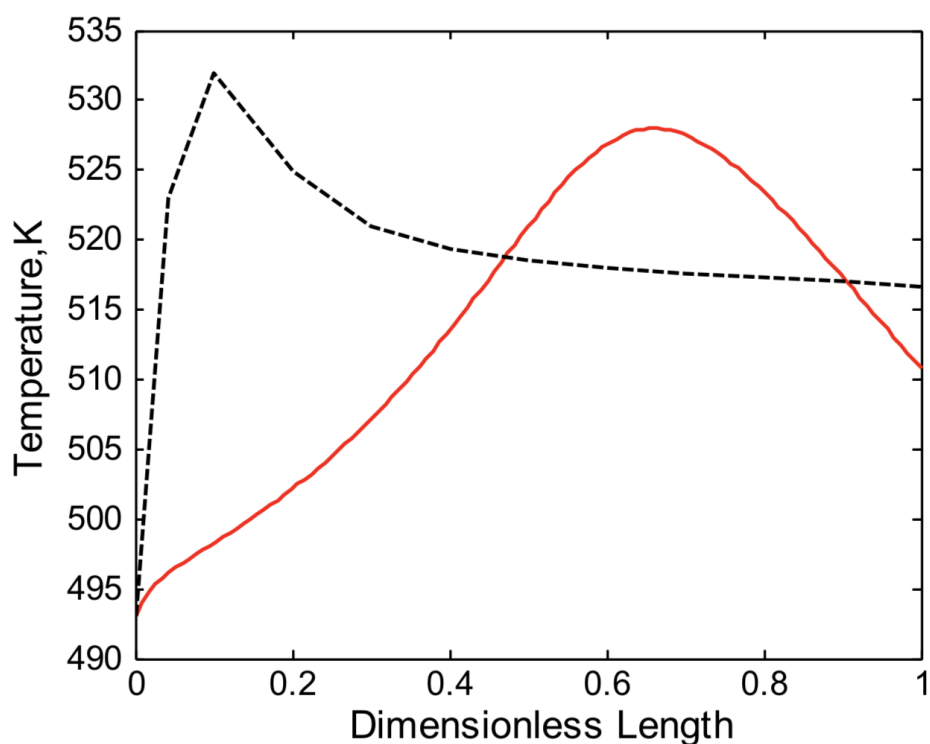


Figure 1.2. Hot-spot formations inside tubular packed bed reactors (adopted from [14,15], as solid line and dashed line, respectively).

facile removal of the exothermic heat and precise regulation of the reaction temperature becomes critical. At this stage microchannel reactors come into the play with their heat and mass transfer rates that are nearly two orders of magnitude higher than those involved in the conventional packed-bed units, offering the unique advantage of operability at near-isothermal conditions. Characteristics dimensions of microchannel reactors are in the range of 1-1000 μm . Catalyst used in these units are either coated to the inner walls of the reactor or packed into the channel volume in particulate form. In some cases the whole reactor can be constructed from the active material. Effective catalyst utilization inside microchannel reactors enhances productivity per unit catalyst amount or reactor volume. The advantage of coating allows the use of high space velocities without suffering from pressure drop. Even though the major

disadvantage seems to be relatively low throughputs due to small channel volumes and catalyst amounts, this can be overcome by simply numbering up the channels to meet the desired capacity. These advantages, more specifically the necessity of precise temperature control has been drawing researchers attention to microchannel reactors about direct DME synthesis reaction system [16].

Microchannel technology has been developed mostly over the last 20 years via the pioneering studies carried out in German Karlsruhe Institute of Technology and Fraunhofer ICT-IMM, and the US Pacific Northwest National Laboratory (PNNL-Battelle). Although common fabrication methodology for microchannel reactors is lamination, 3D-printing is now available as an alternative, enabling realization of the potential in the fine chemical industry for achieving higher yields and selectivities, less by-products with minimum waste and cost. Scaling-up to commercial production is applied by means of parallelization which is much more simpler and cheaper than the traditional scaling-up studies of the conventional units [16].

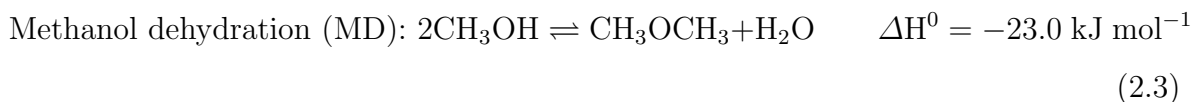
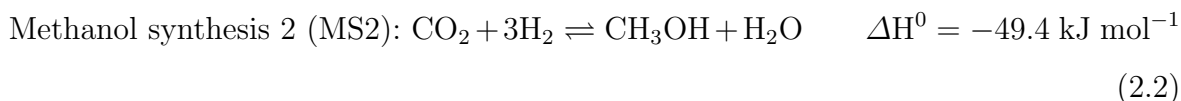
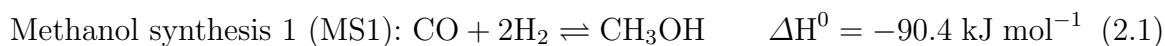
This study focuses on the design considerations on DME production in a wash-coated microchannel reactor by means of a parametric study, making temperature, pressure, inlet velocity, H_2/CO , H_2/CO_2 of CO_2 -containing syngas feed, as well as construction material and wall thicknesses within the reactor the investigated parameters. The aim is to determine the optimum design parameters to acquire high syngas conversion and DME yield. The model is constructed on experimentally obtained global kinetics [15].

The present thesis involves 5 main chapters, including Introduction. In Chapter 2, an extensive literature survey on DME production is provided. In Chapter 3, design parameters of the microchannel reactor, reaction network and mathematical modeling of kinetics are presented. In Chapter 4, results of parametric study are given and discussed in detail. Finally, in Chapter 5, conclusion from the study and recommendations for further work are given.

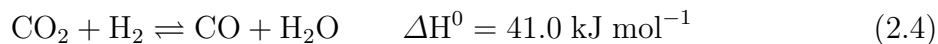
2. LITERATURE SURVEY

2.1. Dimethyl Ether Production

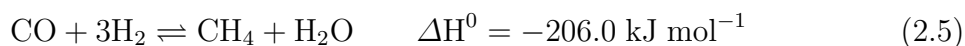
DME is produced from syngas, a mixture of hydrogen and carbon monoxide, which is obtained industrially from fuels, mostly natural gas, either by gasification or steam reforming. DME production involves a series of exothermic equilibrium reactions, namely conversion of syngas to methanol (via Reactions 2.1 and 2.2) and subsequent dehydration of methanol to DME via Reaction 2.3 [4, 8]:



Relative amount of CO_2 in syngas dictates the extent of reverse water-gas shift (RWGS):



Exothermic nature of the methanol synthesis and dehydration reactions inherently causes elevation in reaction temperature. Unless removed by means of cooling, exothermic temperature rise above 573 K causes undesired methane formation via Reaction 2.5 [17]:



Since biofuel production has gained growing importance, numerous studies have been carried out about DME synthesis both experimentally and computationally. DME production can be carried out in two different ways. The first one is called the two-step or indirect route and the other one is called the single-step or direct route (Figure 2.1). In the two-step process methanol is produced in the first reactor, and after purification, it is dehydrated to DME in a secondary reactor. In the relatively new one-step direct process, methanol synthesis and its dehydration into DME take place in the same reactor on a bifunctional or hybrid catalysts [4]. In the following sections, essential information about both indirect and direct synthesis of DME by experimentally and computationally will be presented and key results will be pointed out.

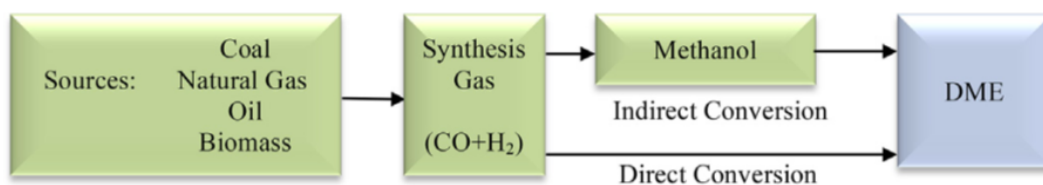


Figure 2.1. DME production diagram [4].

2.1.1. Indirect DME Synthesis

Traditionally, DME is produced in a two-step process since high selectivity of DME can be easily achieved at mild conditions and purification of products are relatively easier compared to direct route. Schematic diagram of the process is given in Figure 2.1 and more detailed methanol dehydration process flowchart is given in Figure 2.2.

Studies regarding indirect DME synthesis from methanol focus mostly on type and properties of the dehydration catalyst. Researchers conduct their experiments in varying temperatures between 380-720 K. Pressure does not have significant effect on process since Reaction 2.3 is in stoichiometric balance. Apart from these studies, some articles handle the process from syngas and this approach introduce new parameters to these studies such as pressure, H_2/CO ratio, CO_2 presence in feed and space velocity in the ranges of 1-100 bar, 0.5-2.5 and 600-3000 h^{-1} , respectively [13]. Reported DME yield

and CO conversion values in these studies are found to vary between 10-100% and 20-97%, respectively. Although typical reaction unit is fixed-bed reactor, DME synthesis by indirect route is studied also in catalytic distillation column [18], catalytic membrane reactor [19] and Platelet Milli-reactor [20]. Methanol dehydration reaction into DME can be achieved using solid acid catalysts. Some of these catalysts investigated in the literature are γ -Al₂O₃ [21–23], HZSM-5 [24,25], HY zeolite supported by modified Cu-Mn-Zn [26], mordenite [27], Nafion and its silicate structured nanocomposites [28] and zeolite SUZ-4 [29].

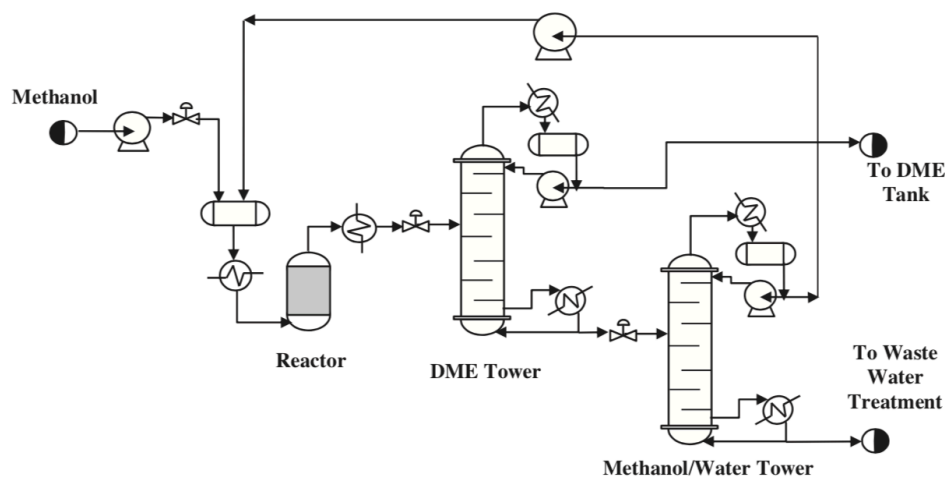


Figure 2.2. DME synthesis from methanol, second part of indirect route [4].

Many articles have been published focusing kinetics of DME synthesis via methanol dehydration on solid-acid catalyst and majority of them state that kinetic mechanism follows either Langmuir-Hinshelwood [30] or Eley-Rideal [31] models in which both DME and water act as reaction inhibitors [18].

Tokay *et al.* [28] investigated alumina impregnated SBA-15 (Al@SBA-15) on DME synthesis from methanol. The authors observed that 80% of methanol was converted into DME without any side product over 573 K. Below that temperature formaldehyde production was observed, as yield of it is 20% at 473 K. Liwei *et al.* [32] prepared a combination of Al₂O₃-HZSM-5 solid acids for methanol dehydration to DME in a fixed-bed reactor. This combination exhibited higher activity than pure Al₂O₃ and possessed higher stability than pure HZSM-5 temperatures below 508 K. At

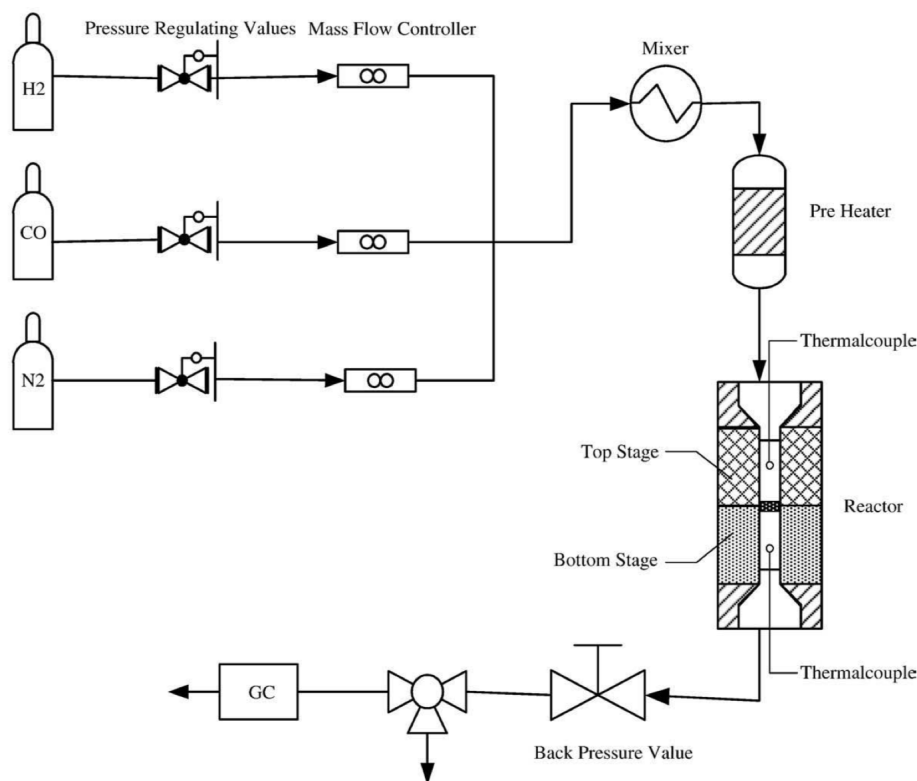


Figure 2.3. Indirect DME synthesis from syngas [4].

this temperature production of DME was reported as $13.5 \text{ g.gcat}^{-1} \text{ h}^{-1}$. Chen *et al.* [13] investigated two-step DME production at different conditions. The study showed that CO₂ introduction to the feed enhanced CO conversion and suggested that optimum values for the reaction system was CO₂/CO ratio of 2, H₂/CO ratio of 4 at 473 K to achieve over 90% CO conversion. Zhu *et al.* [33] studied improved two-step synthesis of DME in a fixed-bed reactor on CuO-ZnO-Al₂O₃ as methanol synthesis catalyst and HZSM-5 as methanol dehydration catalyst. Study states optimum reaction temperatures of the top (methanol synthesis) and bottom (methanol dehydration) stage as 543-553 and 508-518 K, respectively. H₂/CO ratio above 2 lead to increase both CO conversion and DME yield from 10 to 52% and 3 to 21%, respectively. Also, effect of increasing pressure was shown as pressure reaches 8MPa from 3 MPa, CO conversion and DME yield from 30 to 78% and 21 to 63%, respectively.

2.1.2. Direct DME Synthesis and Intensification

The direct route of DME synthesis is performed over either bifunctional or hybrid catalysts. Thermodynamic limitation existing in the indirect route is surpassed since produced methanol is continuously converted into DME. In general, higher CO conversions are achieved in the direct route. Moreover, required investment is relatively lower than that of the indirect route.

Studies regarding the catalysts used in the direct route focus mostly on the impact of the acidic dehydration catalyst on the extent of DME synthesis and investigate the degree of acidity on CO conversion and on product distribution with emphasis on DME selectivity and yield. In this respect, catalysts with acidic properties such as γ -Al₂O₃ [17, 34, 35], SiO₂-Al₂O₃ [36, 37] and zeolites such as HZSM-5, H-Y, H-Beta and H-Ferrierite [38–41] are studied at reaction temperature, molar syngas ratio (H₂/CO), pressure and residence time ranges of 513–553 K, 0.5–2, 1–70 bar and 3–8 kgcat.h kmol⁻¹, respectively. These conditions are reported to deliver CO conversions between 53–95% and DME yields between 34–52%. The studies also emphasize that relative amounts of synthesis and dehydration catalysts are dictated by the properties of the latter and change between 1:1 and 3:1 (Cu-ZnO/Al₂O₃:acidic catalyst by mass). Even though CO₂ can exist in the syngas mixtures obtained from hydrocarbon reforming/gasification routes, the impact of its existence in the feed on DME synthesis is investigated in a limited number of studies that commonly use Cu-ZnO/Al₂O₃ as the synthesis catalysts and γ -Al₂O₃ [42], ZSM-5 [43] and HZSM-5 [44, 45] as the dehydration catalysts. It is reported that at reaction temperatures, molar H₂/CO₂ ratios and pressures between 513–543 K, 2–10 and 30–40 bar, respectively, CO₂ conversions of 15–50% and DME yields of 9–25% are obtained [8]. Further details regarding the synthesis, characterization and performance of individual and hybrid synthesis and dehydration catalysts can be found in the excellent review of Saravanan *et al.* [8].

In addition to the nature of the catalysts, rate of removal of the heat released by Reactions 2.1–2.3 from the catalyst bed dictates the success of the direct synthesis approach, which ideally calls for the need of isothermal conditions. Deviations

from isothermal behavior cause the reactions to be limited by thermodynamics and subsequent reduction in DME yield and CO conversion. Importance of temperature regulation increases further by the presence of CO₂ in synthesis gas. RWGS (Reaction 2.4), favored with CO₂ in the feed and at high temperatures caused by exothermic heat generation, increases the amount of steam which shifts dehydration in the direction of methanol formation. The resulting methanol suppresses syngas consumption via reversal of the methanol synthesis. Steam also accelerates deactivation of methanol synthesis and dehydration catalysts via their sintering at temperatures in excess of 573 K [8, 34, 46]. Due to these problems associated with CO₂, a well-known greenhouse gas, its use as a feedstock in production of DME, a value-added product, becomes difficult. Even though the rate of heat transfer on the catalyst bed is known to be a strong function of reactor architecture, it is investigated and quantified only in a few studies in the literature. Hu *et al.* [47] studied direct DME synthesis in a microchannel reactor packed with a physical mixture of commercial methanol synthesis and dehydration catalysts in particulate form. Authors reported DME yields 3 times higher than their commercial counterparts with much slower rates of catalyst deactivation, and linked these findings with the improved temperature control enabled by the miniaturized reactor dimensions. In a series of studies, Hayer *et al.* [48–50] integrated cooling function to the microchannel reactor packed with physical mixtures of particulate catalysts for methanol synthesis (Cu–ZnO/Al₂O₃) and dehydration (γ -Al₂O₃ and HZSM-5) and studied the effects of composition, feed rate, temperature and pressure of syngas and inlet temperature of the coolant on CO conversion and DME selectivity by means of experimentation and mathematical modeling. They showed effective intensification of direct DME synthesis by means of coupling heat exchange and catalytic reaction functions at micro scales. In another study, McBride *et al.* [51] demonstrated the importance of catalyst positions on heat transfer rate and temperature distribution. In these studies, however, the catalysts are in particulate form only and the syngas feed does not include CO₂. For various reactions it is reported that more efficient use of the catalysts is possible by coating them as thin layers to the inner walls on the microchannel rather than packing them in particulate form [52, 53]. At this point, wall-coated microchannel reactors come into play with their heat transfer rates

that are 10^2 higher than those of their packed-bed counterparts and offer near ideal effectiveness of catalyst use together with notably increased productivities per unit catalyst amount or reactor volume [54–57]. These units, characterized by channels with hydraulic diameters in the range of 10^{-6} – 10^{-2} m and washcoated catalyst layers thickness below 1×10^{-4} m, are precisely machined from mostly metallic substrates which, combined with surface area-to-volume ratios in the order of $10^4 \text{ m}^2 \text{ m}^{-3}$, favor heat transport and precise regulation of temperature to the ideal interval demanded for peak catalyst effectiveness [58, 59]. Moreover, ease of cooling integration allows microchannel units to operate under isothermal conditions allowing precise balance of the kinetic and thermodynamic effects [60, 61]. This study involves a quantitative parametric study for providing insight into the potential benefits of heat exchange integrated microchannel reactor operation in direct DME synthesis from synthesis gas involving CO_2 , which further increases the detrimental effects of thermodynamics and calls for the requirement of precise temperature control of the catalyst bed. Lack of studies regarding investigation of wall-coated, multifunctional microchannel reactors in the conversion of CO_2 containing syngas to DME forms the motivation of the present study.

3. MATHEMATICAL MODELING

3.1. Details of the Microchannel Reactor

Schematic representation of the heat-exchange integrated microchannel reactor is presented in Figure 3.1. The multichannel unit involves periodically located parallel groups of reaction and cooling channels that are physically separated by a metallic wall. Each channel is 7.5×10^{-2} m long and has a rectangular cross section with dimensions of 3×10^{-4} m (H) \times 6×10^{-4} m (W). Rectangular cross-section is selected on the basis of its relative ease of micromachining [62], while the choice of the cross-sectional dimensions is based on the balance between transport rates, which increase at smaller hydraulic diameters due to cross-sectional shape dependent asymptotic Nu and Sh numbers, and pressure drop, which becomes elevated in narrower channels [58, 59, 63]. A uniform, physical mixture of Cu-ZnO/Al₂O₃ and γ -Al₂O₃ catalysts (with a mass ratio of 1:1) is considered to be washcoated to the 6×10^{-4} m (W) \times 7.5×10^{-2} m (L) planes facing each other at the interior of each reaction channel.

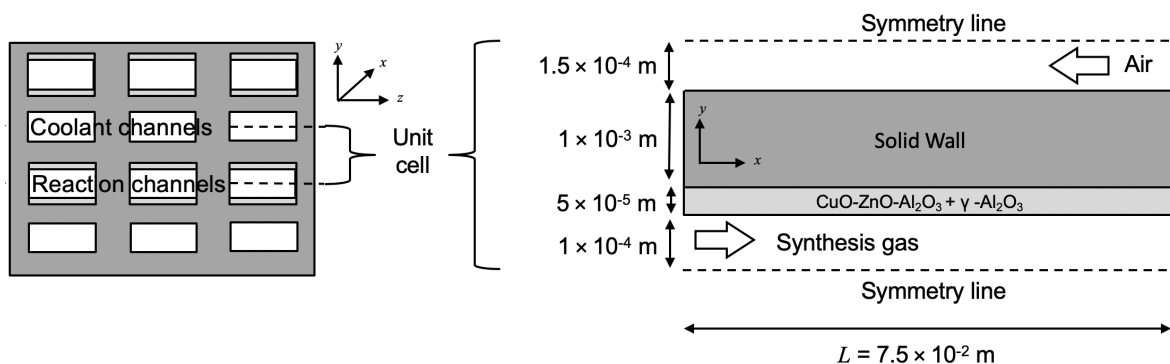


Figure 3.1. Simplified (not to scale) illustrations of the intensified, microchannel DME synthesis reactor (left) and the unit cell (adopted from [64])

Particular partitioning of the reaction and cooling channels allows neglecting the inter-channel heat transfer in the z -direction, i.e. between identical channels. This assumption allows elimination of one spatial dimension and representation of the operation in two dimensions, x and y . The impact of this simplification on the

heat transfer properties of the reaction channel is studied by means of calculating the spatial evolution of the Nu numbers calculated by two- and three-dimensional models for ethylene epoxidation, which is very similar to DME synthesis in terms of the degree of exothermicity of the reactions [64]. Comparison of the Nu numbers showed that the difference between the models remains negligible [64], allowing safe use of two-dimensional model in the present study. Periodic grouping of the channels also allows the so-called unit cell to be the representative geometry of the two-dimensional multichannel unit (Figure 3.1). The unit cell representation is based on the cancellation of the heat fluxes in y -direction on the symmetry lines of the reaction and cooling channels. Further details regarding the basis and details of the unit cell simplification can be found elsewhere [64–66].

3.2. Reaction Network and the Kinetic Model

DME synthesis from syngas is considered to take place via the independent methanol synthesis and dehydration reactions (Reactions 2.1-2.3) on a mixture of Cu-ZnO/Al₂O₃ and γ -Al₂O₃ catalysts coated to the inner walls of the reaction channel. Since RWGS (Reaction 2.4) depends on the combination of Reactions 2.1 and 2.2, it is not considered in the model reactions. Moreover, Reaction 2.5 is not included in the simulated reaction network due to the facts that formation of methane and other paraffins during DME synthesis on Cu-ZnO/Al₂O₃ and γ -Al₂O₃ mixture remains negligible below 573 K [17] and the reaction temperature will be kept well below this value due to integrated cooling. Similarly, 573 K is specified as the limit below which agglomeration of Cu nanoparticles on Cu-ZnO/Al₂O₃ and pore closure on γ -Al₂O₃ driven by hydrothermal sintering becomes negligible [42]. In addition, possibility of deposition of carbonaceous species is reported to remain negligible mainly by the reversal of Boudouard reaction ($2CO = CO_2 + C(s)$, $\Delta H^0 = -172 \text{ kJ mol}^{-1}$) in the presence of CO₂ in the feed [42, 46]. Based on these experimental evidences, both catalysts are assumed to run at their active states without being subject to deactivation. In the light of these assumptions, the following kinetic model adapted from Hu

et al. [15] is used for quantifying the rates of Reactions 2.1-2.3:

$$r_{MS1} = \frac{k_{MS1}f_{CO}f_{H_2}^2(1 - \beta_{MS1})}{(1 + K_{CO}f_{CO} + K_{CO_2}f_{CO_2} + K_{H_2}f_{H_2})^3}, \quad \beta_{MS1} = \frac{f_{CH_3OH}}{K_{D,MS1}f_{CO}f_{H_2}^2} \quad (3.1)$$

$$r_{MS2} = \frac{k_{MS2}f_{CO_2}f_{H_2}^3(1 - \beta_{MS2})}{(1 + K_{CO}f_{CO} + K_{CO_2}f_{CO_2} + K_{H_2}f_{H_2})^4}, \quad \beta_{MS2} = \frac{f_{CH_3OH}f_{H_2O}}{K_{D,MS2}f_{CO}f_{H_2}^3} \quad (3.2)$$

$$r_{MD} = \frac{k_{MD}f_{CH_3OH}(1 - \beta_{MD})}{(1 + \sqrt{K_{CH_3OH}f_{CH_3OH}})^2}, \quad \beta_{MD} = \frac{f_{CH_3OH}f_{H_2O}}{K_{D,MD}f_{CH_3OH}^2} \quad (3.3)$$

Methanol synthesis reactions (MS1 and MS2) are considered to run on Cu–ZnO/Al₂O₃, whereas methanol dehydration (MD) is driven by γ -Al₂O₃ [15]. Constants needed to predict temperature dependence of the parameters existing in Equations 3.1–3.3 are presented in Table 3.1:

Table 3.1. Temperature dependence of the parameters used in the kinetic model
(adapted from Hu *et al.* [15])

$k_{rxn}, K_i = A \cdot \exp(B/(RT))$	A	B
k_{MS1}	1.2×10^3	-43723
k_{MS2}	2.8×10^1	-30253
k_{MD}	5.8×10^1	-24984
K_{CO}	8.252×10^{-4}	30275
K_{CO_2}	2.1×10^{-3}	31846
K_{H_2}	1.035×10^{-1}	-11139
K_{CH_3OH}	1.726×10^{-4}	60126

The rate laws are expressed in terms of the fugacity of the components existing in the mixture. These terms can be related to pure component fugacities by means of

the Lewis law given through the expression below [67]:

$$f_i = y_i f_{pure,i}, \quad f_{pure,i} = \exp\left[\left(b_i - \frac{a_i}{RT}\right) \frac{p}{RT} + \ln p\right] \quad (3.4)$$

The van der Waals coefficients needed to predict temperature dependence of the fugacity terms existing in Equations 3.1–3.3 are given in Table 3.3:

Table 3.2. The van der Waals coefficients used for evaluation of Equation 3.4
(adapted from [67])

Species(<i>i</i>)	a_i (<i>bar L</i> ² <i>mol</i> ⁻²)	b_i (<i>L mol</i> ⁻¹)
CO	1.472	0.03948
H₂	0.2453	0.02651
CO₂	3.658	0.04286
H₂O	5.537	0.03049
CH₃OH	9.472	0.06584
CH₃OCH₃	8.69	0.07742
CH₄	2.3	0.04301

The kinetic model necessitates the prediction of equilibrium constants of Reactions 2.1–2.3 as a function of temperature via the molar Gibbs free energy of the particular reaction:

$$K_{D,rxn} = \exp(-\Delta G_{rxn}/RT), \quad rxn = MS1, MS2, MD \quad (3.5)$$

Gibbs free energy of formation of reactive species (CO, H₂, CO₂, H₂O, CH₃OH and CH₃OCH₃), required to calculate Gibbs free energy of the reaction via Equation 3.6, can be estimated by the temperature dependent expressions presented in Equations

3.7–3.9 and by the use of accompanying constants given in Table 3.3:

$$\Delta G_{rxn} = \sum_{i=products} n_i G_{f,i} - \sum_{i=reactants} n_i G_{f,i} \quad (3.6)$$

$$\frac{G_{f,i}}{RT} = \frac{H_{f,i}}{RT} - \frac{S_{f,i}}{R} \quad (3.7)$$

$$\frac{H_{f,i}}{RT} = a_1 + a_2 \frac{T}{2} + a_3 \frac{T^2}{3} + a_4 \frac{T^3}{4} + a_5 \frac{T^4}{5} + \frac{b_1}{T} \quad (3.8)$$

$$\frac{S_{f,i}}{R} = a_1 \ln T + a_2 T + a_3 \frac{T^2}{2} + a_4 \frac{T^3}{3} + a_5 \frac{T^4}{4} + b_2 \quad (3.9)$$

Table 3.3. Constants needed for the estimation of Gibbs free energy of formation of the species (adapted from [68])

Species	a_1	$a_2(\times 10^3)$	$a_3(\times 10^6)$	$a_4(\times 10^9)$	$a_5(\times 10^{12})$	$b_1(\times 10^{-4})$	b_2
CO	3.58	-0.61	1.02	0.91	-0.90	-1.43	3.51
H ₂	2.34	7.98	-19.5	20.2	-7.38	-0.092	0.68
CO ₂	2.36	8.98	-7.12	2.46	-0.14	-4.84	9.90
H ₂ O	4.20	-2.04	6.52	-5.49	1.77	-3.03	-0.85
CH ₃ OH	5.72	-15.2	65.2	-71.1	26.1	-2.56	-1.50
CH ₃ OCH ₃	5.31	-2.14	53.1	-62.3	23.1	-2.40	7.13
CH ₄	5.15	-13.7	49.2	-48.5	16.7	-1.02	-4.64

3.3. Reactor Operation, Overview of the Parametric Study and Numerical Solution

Default operation of the unit cell, the representative geometry of the multichannel reactor block, involves counter-current feeding of coolant (air) and the reactive stream, which is assumed as a homogeneous mixture of CO, CO₂, H₂ and N₂ (balance gas), both at 50 bar and 508 K. Syngas composition quantified by the molar inlet H₂/CO and H₂/CO₂ ratios set to 2.5 and 10, respectively, as default values. The ranges of operating parameters, namely, inlet pressure, temperature, H₂/CO and H₂/CO₂ ratios are determined as 20–60 bar, 493–508 K, 2.5–4.0 and 5–12, respectively, in the light of condition ranges employed in the literature [8]. In all simulations, feed temperature and pressure of air are taken as the same with those of syngas. Thickness of the solid wall separating the channels is investigated between $1\text{--}2 \times 10^{-3}$ m, with 1×10^{-3} m being selected as the default value. Stainless steel (316 grade) is used as the standard wall material among the other options, namely cordierite and FeCrAl. The materials are selected on the basis of their availability and compatibility with several micromachining techniques and their wide use in the construction of catalytic microchannel reactors [54, 62]. The effect of a parameter on reactor performance is studied by changing its value/attribute within its specified range, while keeping the others at their defaults. It is assumed that each channel in the multichannel reactor has exactly the same inlet flow rate and the reactor block operates adiabatically that allows neglect of heat transfer across the outermost boundaries. The former assumption necessitates precise uniformity of the channel dimensions and thickness of the coated catalyst layer together with the lack of deposition of carbonaceous species so that the main reactive stream is partitioned equally to the channels. As mentioned in Section 3.2, conditions of DME synthesis pertinent to the present study do not favor coking. The existing techniques of machining and washcoating of microchannels, however, can lead to some minor fluctuations in the catalyst layer and cross-sectional channel dimensions along the x-direction (Figure 3.1). Even though such fluctuations will have limited impact on the reactor performance, they can be captured by simulating the multichannel block with the numerical techniques employed in the present study, but at the expense of significant elevation of the computation load. Therefore, the impact of dimensional

variations on reactor performance are intentionally kept out of the scope of the work.

In the light of the assumptions above, steady-state operation of the multichannel unit can be described by the simultaneous occurrence of (i) transport of momentum heat and mass in fluid phases of both channels, (ii) reactive transport within porous catalyst layer and (iii) conductive heat transfer along the solid wall within the domain of the unit cell presented in Figure 3.1.

Table 3.4. Model equations used to simulate DME synthesis within the unit cell (Figure 3.1)(adapted from [69])(FP: fluid phases in reaction and cooling channels, CWP: catalytic washcoat phase in reaction channel, SW: solid wall between the channels)

Continuity equation	$\nabla \cdot (\rho_m \vec{v}) = 0$
Momentum eq.(FP)	$\nabla \cdot (\rho_m \vec{v}\vec{v}) = \nabla p + \nabla \cdot [\mu_m (\nabla \vec{v} + (\nabla \vec{v})^\gamma - \frac{2}{3}(\nabla \cdot \vec{v})\mathbf{I})]$
Momentum eq. (CWP)	$\nabla \cdot (\rho_m \vec{v}\vec{v}) = \vec{F} - \nabla p + \nabla \cdot [\mu_m (\nabla \vec{v} + (\nabla \vec{v})^\gamma - \frac{2}{3}(\nabla \cdot \vec{v})\mathbf{I})]$ $\vec{F} = -(\frac{\mu_m}{\alpha} \vec{v} + \frac{C_2}{2} \rho_m \vec{v} \vec{v})$ $\alpha = \frac{d_p^2}{150} \frac{\epsilon_{cat}^3}{(1 - \epsilon_{cat})^2}; C_2 = \frac{3.5}{d_p} \frac{(1 - \epsilon_{cat})}{\epsilon_{cat}^3}$
Species mass eq. (FP)	$\nabla \cdot (\mu_m \vec{v} Y_i) = -\nabla \cdot \vec{J}_i; \quad \vec{J}_i = -\rho_m D_{i,m} \nabla Y_i$
Species mass eq. (CWP)	$\nabla \cdot (\mu_m \vec{v} Y_i) = -\nabla \cdot \vec{J}_i + M_i R_i; \quad \vec{J}_i = -\rho_m D_{eff,i,m} \nabla Y_i$ $R_{CO} = -r_{MS1}; \quad R_{H_2} = -2r_{MS1} - 3r_{MS2}$ $R_{CH_3OH} = r_{MS1} + r_{MS2} - 2r_{MD}; R_{CH_3OCH_3} = r_{MD}$ $R_{CO_2} = -r_{MS2}; \quad R_{H_2O} = r_{MS2} + r_{MD}$
Energy eq. (FP)	$\nabla \cdot (c_{p,m} \vec{v} T) = \nabla \cdot (k_m \nabla T)$
Energy eq. (CWP)	$\nabla \cdot (c_{p,m} \vec{v} T) = \nabla \cdot (k_{eff,m} \nabla T) + \sum_{rxn} (-\Delta H_{rxn})(r_{rxn})$
Energy eq. (SW)	$\nabla \cdot (k_w \nabla T) = 0$

These phenomena can be described mathematically by the set of model equations presented in Table 3.4. The linear inlet velocities of the reactive stream and air, both

assumed to be of Newtonian type fluids, are set to 0.1 and 10 m s⁻¹, respectively, and make the flow regime laminar as characterized by the Reynolds numbers (Re) of 1.4×10^{-1} and 1.6×10^1 respectively. Feed velocity of the syngas is based on the GHSV of 16080 Nml gcat⁻¹ h⁻¹ which is in accordance with those involving DME synthesis on the same catalyst bed considered in the present study [9, 70]. Under these conditions and the channel geometries defined in Section 3.1, pressure drop in both channels remained below 1%, which is in alignment with those of the microchannel units having similar dimensions [71, 72]. Boundary conditions needed for the numerical solution involves the definition of temperatures, linear velocities and species mass fractions at the channel inlets and exit gauge pressures at the channel outlets. Condition at the catalyst layer–fluid interface is integrated to the model by means of continuity of heat and species mass fluxes, and velocity. Material and heat fluxes across and components of velocities normal to the symmetry lines are taken to be zero. The remaining boundaries in the unit cell are set to involve no-slip conditions. Gas-phase reactions are neglected, as they remain slower than those running on the catalyst layer, which is valid even for high-temperature ($> \sim 1000$ K) processes such as catalytic oxidation of methane [73].

The model equations involve fluid properties such as viscosity, density, molecular weight, heat capacity, thermal conductivity of and species diffusivity within the reactive mixture, effective thermal conductivity of the reactive mixture and species diffusivity within the pores of the catalyst layer, Knudsen and binary diffusivities, all of which can be estimated by the pertinent correlations compiled and reported elsewhere [64, 69]. The 5×10^{-5} m thick catalyst layer is modeled as a homogeneous porous medium composed of a uniform physical mixture of Cu–ZnO/Al₂O₃ and γ -Al₂O₃ having a mass ratio of 1:1. The selected washcoat thickness ensures minimization of intra-layer heat and mass transport resistances and is reported to remain mechanically stable in a number of applications [58]. Tortuosity, porosity, thermal conductivity and density of the catalyst layer are taken as 1.64, 0.61, 24.2 W m⁻¹ K⁻¹ and 2366 kg m⁻³, respectively, while the average diameter of the pores, assumed to have cylindrical cross-sections, is set to 1.14×10^{-8} m [9]. Difference between the outcomes of the comparative simulations remained below 1% when the physical properties of the bed are represented either by

those of Cu–ZnO/Al₂O₃ or of γ -Al₂O₃. In this respect, properties of Cu–ZnO/Al₂O₃ are adapted as those of the mixed catalyst layer. Permeability and inertial resistance of the coated catalyst layer, both of which exist in the momentum conservation equation for the washcoat phase in Table 3.4, are calculated by equalizing particle diameter to the layer thickness. Total mass of catalyst layer coated to both surfaces of one reaction channel is calculated as 1.07×10^{-5} kg. Owing to the fact that the maximum change in the reaction temperature remains well below 20 K in the simulations (Section 4), temperature dependence is ignored in evaluating the fluid properties which is carried out at the particular feed temperature to decrease computation time. Such a simplification is reported to have negligible changes in the outcomes of oxidation and steam reforming of methane, both simulated in a catalytic microchannel reactor at temperatures in excess of ~ 850 K [74], which is much higher than those (i.e. < 300 K) involved here.

Simultaneous solution of the mathematical model which is composed of a set of non-linear partial differential equations (Table 3.4) is carried out by the finite volume method executed under ANSYS (version 19.2) platform. The solution domain (i.e. the unit cell) is discretized by rectangular cells via the Gambit software (version 2.3.16) to give a total of 4.05×10^5 nodes, with 2.6×10^4 cells for the half reaction channel, 1.3×10^4 cells for the porous catalyst layer, 3.9×10^4 cells for the half cooling channel and 2.6×10^5 cells for the solid wall. The kinetic model composed of the rate expressions (Equations 3.1–3.3) and the auxiliary equations (3.4–3.9) together with the pertinent correlations for the estimation of fluid properties are integrated with ANSYS structure in the form of user-defined functions. Numerical solution is carried out on a HP Z440 workstation with 32 GB of memory. Every simulation reported in this study is run at least twice to check the reproducibility of the results, which are found to deviate only after the second digit following the decimal point. Impact of the discretization scheme is also investigated by further refining of the mesh, i.e. increasing the number of grid points, which ended up with only $< 1\%$ differences in the temperature profiles obtained under all combinations of operating conditions. The impact of each parameter on reactor performance is quantified in terms of temperature profiles obtained at the catalyst–fluid interface of the reaction channel and CO conversion together with yields of DME,

CH_3OH and H_2O . CO conversion is defined as the ratio of moles of CO converted to the moles of CO fed, while the yield of species i is defined as the ratio of moles of species i in the product mixture to the moles of CO at the inlet. In these definitions, the term “moles” refer to the pertinent molar flow rate that is surface-averaged on the channel cross section.

4. RESULTS AND DISCUSSION

4.1. Validation of the Reactor Model

Capability of the mathematical model in capturing the real reactor performance is carried out prior to its use in the simulation of intensified DME production from CO₂-containing syngas. The experimental data is adapted from the study of Hayer *et al.* [49] which involves DME production from syngas fed with molar percent composition of H₂:CO:CO₂:N₂:CH₄ = 42:42:5:5:6 within 483–573 K temperature, 10–50 bar pressure and 4.5×10^3 – 6×10^4 Nml gcat⁻¹ h⁻¹ gas-hourly space velocity (GHSV) ranges into a heat-exchange microchannel reactor packed with 1:1 (by mass) physical mixture of CuO–ZnO–Al₂O₃ and γ -Al₂O₃ catalysts in particulate form. Under these conditions near-isothermal DME synthesis free of mass and heat transport limitations is demonstrated [49].

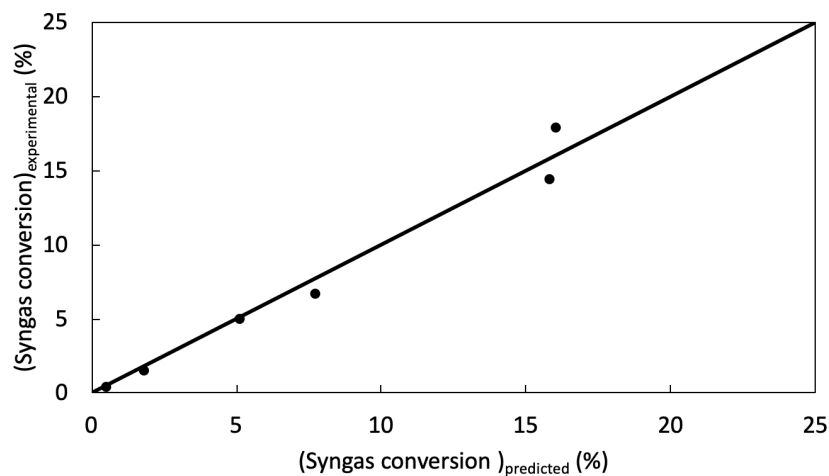


Figure 4.1. Comparison of the experimental and predicted syngas conversions.

Experimental data is taken from [49].

In this respect, the experimental data can be used to test the mathematical model for the proposed wall-coated microchannel reactor which inherently disables transport resistances even in very exothermic reactions such as ethylene oxide synthesis [75]. Outcomes of the experiments run at 483, 503 and 523 K, 50 bar and GHVSs of 4.5×10^3 and

1.5×10^4 Nml gcat⁻¹ h⁻¹, all of which are very close to the conditions employed in the present study, are compared with those computed via the model explained in Section 3, and reported in the parity plot presented in Figure 4.1 in terms of per cent conversion of syngas (i.e. CO and H₂). The results show that experimental and predicted conversions satisfactorily agree with each other and deviate within the range of 3–14%. This finding justifies the kinetic expressions and the complementary thermodynamic relationships together with the unit cell approach and the accompanying assumptions, all of which are the building blocks of the mathematical model that will be used to quantify intensified DME synthesis in the following sections.

4.2. Effect of Syngas Feed Temperature

The effect of feed temperature of syngas on the spatial evolution of the reaction channel temperature, reaction rates, CO conversion and yields of methanol and steam are presented in Figure 4.2. Four different feed temperatures are studied in the 493–508 K range with increments of 5 K, while the other parameters are kept at their defaults given in Section 2.3. All cases involve a common trend of reaction temperature which initially increases rapidly as the syngas feed contacts with the catalyst layer and then keeps on decreasing along the channel due to the integrated counter-current cooling (Figure 4.2a). Despite the fast temperature ramp, the maximum value of the gradient between the inlet and the hot-spot remains at 9 K, which is significantly below 40 K reported for externally cooled tubular reactors packed with the same catalysts (i.e. 1:1 physical mixture of Cu-ZnO/Al₂O₃ and γ -Al₂O₃) and run under equivalent operating conditions [14, 15]. Space time yields (STY) of conventional DME synthesis units and the proposed intensified microchannel reactor are compared at similar conditions. The difference is related with the improved heat transfer rates of wall-coated microchannel reactors and clearly shows their capability in minimizing the negative impacts of hot-spots such as catalyst deactivation. The intensified reactor is also compared with its conventional counterparts on the basis of space time yield (STY), defined as the ratio of the mass flow rate (tons h⁻¹) of DME produced per reactor volume confining the catalyst bed. For this purpose, STY is comparatively calculated for a packed-bed type,

directDME synthesis reactor and for the air-cooled microchannel reactor, both of which involve the same catalysts mixed with identical proportions. Hu *et al.* [15] reported that industrial packed-bed reactor running at temperature and pressure ranges of 493-523 K and 23-40 bar, respectively, can perform to deliver STYs in between 0.11 and 0.13 $\text{tons}_{\text{DME}_{\text{produced}}} \text{m}^{-3} \text{h}^{-1}$. Microchannel reactor in the present study, on the other hand, is simulated to run at STYs between 0.10-0.24 $\text{tons}_{\text{DME}_{\text{produced}}} \text{m}^{-3} \text{h}^{-1}$ at conditions of 503-508 K and 20-50 bar on the basis of reaction channel volume. This comparison reveals that, in addition to its capability of suppressing hot-spot formation, the heat-exchange integrated microreactor can improve volumetric productivities observed in the conventional units.

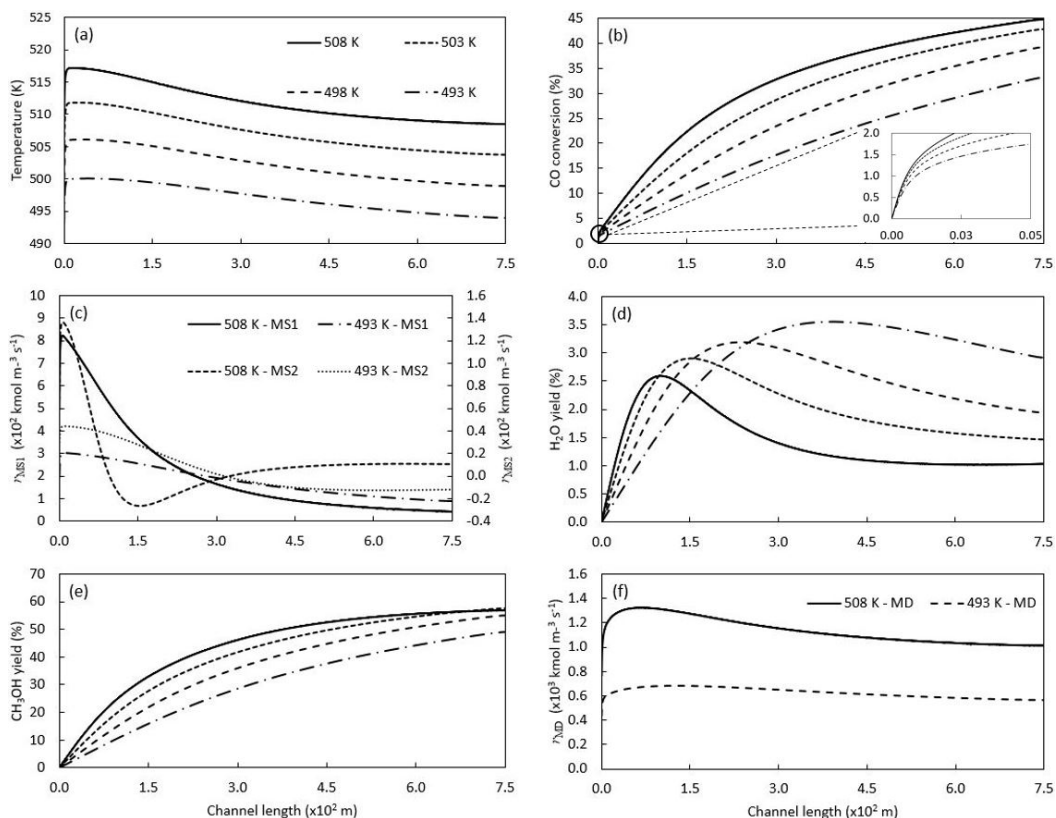


Figure 4.2. Evolution of (a) temperature, (b) CO conversion, (c) rates of methanol synthesis reactions, yields of (d) steam and (e) methanol, and (f) rate of methanol dehydration along the reaction channel at different syngas feed temperatures.

The root cause of the instant temperature rise at the channel inlet can be explained by the 2% CO conversion observed at the same location (Figure 4.2b, inset) via

Reaction 2.1 and is in well-alignment with the fast nature syngas-to-methanol conversion over Cu-ZnO based catalysts. After its instant elevation, CO conversion increases along the channel with a rate that is inversely proportional with the feed temperature. This pattern, together with the rate of decrease in temperature becoming more notable at hotter feeding, can be explained with the opposing effect of thermodynamics. As methanol synthesis reactions are exothermic, they become slower or even reversed depending on the extent of temperature rise. This qualitative fact is quantified by calculating the reaction rates along the channel lengths for the lowest and highest inlet temperatures, 493 K and 508 K, respectively, as presented in Figure 4.2c. Analysis of the reaction rates reveal that, compared to methanol formation by CO₂ hydrogenation, the CO hydrogenation route is faster and always proceeds in forward direction, as revealed by its positive rates along the channel. Moreover, faster decline of its rate at higher feed temperatures due to pronounced impacts of thermodynamic limitations provides fundamental explanation of temperature and CO conversion trends at 508 K feeding.

In contrast with that of Reaction 2.1, direction of CO₂ hydrogenation (Reaction 2.2) is found to change along the channel length. After a sharp increase upon feeding at 508 K, its rate is found to decline, followed by reversal at channel lengths between $1-3.5 \times 10^{-2}$ m, after which positive rates are observed again. As expected, feeding at the lowest temperature of 493 K decreases the rates of both reactions, with Reaction 2.2 having slightly negative values at the second half of the channels. The extent of CO₂ hydrogenation can be visualized better by analyzing the spatial changes in the yields of steam and methanol presented in Figures 4.2d and 4.2e, respectively. The H₂O yield trend calculated at 508 K feeding is in perfect alignment with the rate of Reaction 2.2, which predicts an early maximum at the yield of 2.5%, followed by a decline corresponding to H₂O consumption due to reversal of Reaction 2.2 until 3.5×10^{-2} m, above which H₂O formation is again promoted, but to a much lesser extent due to the slightly positive rates. Interestingly, higher yields of H₂O up to 3.5% are obtained by lowering feed temperature to 493 K. This finding is in alignment with the corresponding CO₂ hydrogenation rate that changed less but remained always above zero in the first half of the channel. Comparison of CO conversion and methanol yields (Figures 4.2b

and 4.2e) at 508 K feeding shows that the latter increases faster than CO conversion in the channel upstream due to the contribution of Reaction 2.2 to methanol yield, whose rate of increase, however, gets significantly lowered in the channel downstream due suppression of CO₂ hydrogenation. Figure 4.2f shows the rates of methanol dehydration are at least 10 times less than those of the synthesis routes. After a characteristic initial boost aided by the immediate abundance of methanol, dehydration rate is found to proceed with a trend in alignment with the particular reaction temperature. As expected, DME yields increase with feed temperature and reach up to 3.6% (Table 4.1) which is found to be in alignment with the literature studies involving operating conditions similar to the ones used in the present study [9, 17, 42].

Table 4.1. DME yield obtained as functions of operating conditions

Parameter	Value	DME yield (%) or molar flow rate ($\times 10^9 \text{ mol s}^{-1}$)
T (K)	493, 498, 503, 508	2, 2.5, 3.1, 3.6
P (bar)	20, 30, 40, 50, 60	2.2, 2.5, 2.8, 3.1, 3.3
H₂/CO	2.5, 3.5, 4	8.42, 7.86, 7.64
H₂/CO₂	5, 7.5, 10, 12	3.1, 3.5, 3.6, 3.6
Inlet syngas flow rate ($\times 10^1 \text{ m s}^{-1}$)	1, 2, 3	8.42, 11.3, 14.1
Wall thickness ($\times 10^3 \text{ m}$)	1, 1.4, 1.6, 2	3.6, 3.6, 3.7, 3.7
Wall material	Steel, Cordierite, FeCrAl	3.6, 3.5, 3.6
Flow partitioning	Counter-current, co-current	3.6, 3.9

Steam is an undesired intermediate in DME synthesis as it accelerates sintering and thermodynamically hinders CO₂ conversion in Reaction 2.2 and DME synthesis in Reaction 2.3. In this respect, feeding syngas at 508 K should be preferred as, compared with the lower inlet temperatures, it minimizes formation of H₂O while favors methanol production, both factors which lead to increased DME yields.

4.3. Effect of Syngas Feed Pressure

The effect of inlet pressure of syngas on the spatial evolution of the reaction channel temperature, reaction rates, CO conversion and yields of methanol and steam are presented in Figure 4.3. Five different feed pressures are studied in the 20–60 bar range with increments of 10 bar, while the other parameters are kept at their defaults given in Section 3.3. Higher pressures lead to increased reaction temperatures, as evident from the profiles in Figure 4.3a. This finding is in accordance with the Le Chatelier’s principle of thermodynamic promotion of a gas–phase reaction to the side with lower number of moles of species. This rule holds for promotion of methanol synthesis via Re-

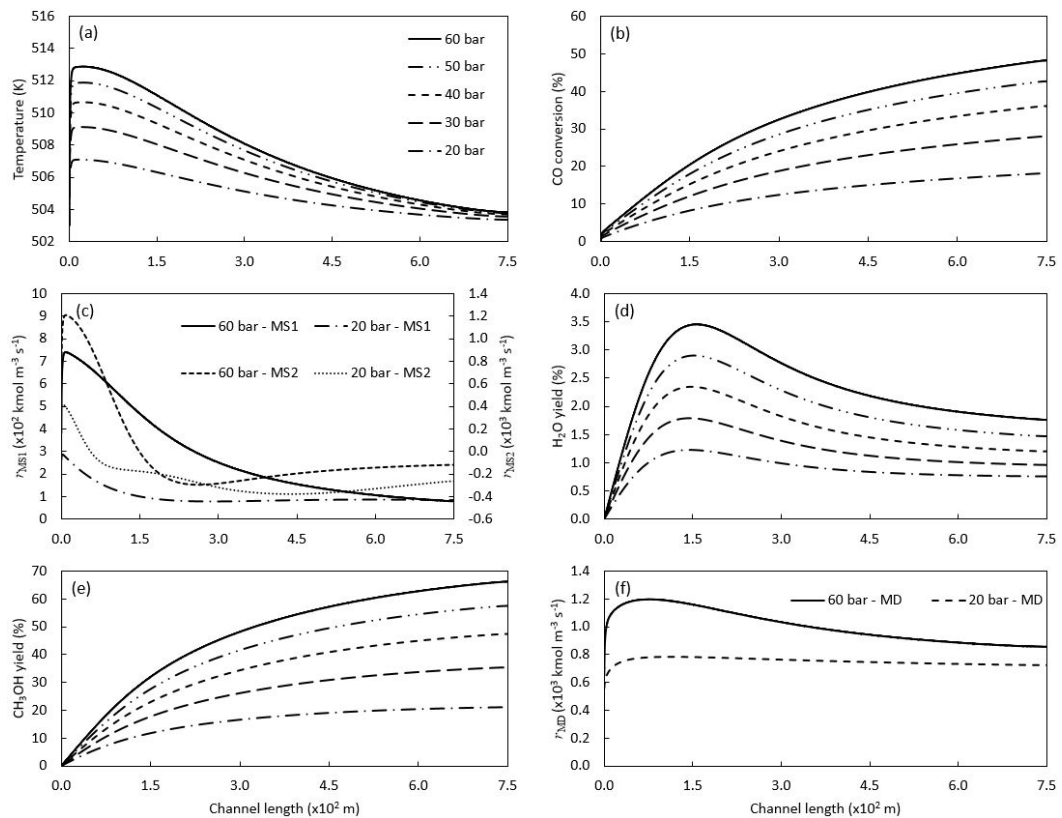


Figure 4.3. Evolution of (a) temperature, (b) CO conversion, (c) rates of methanol synthesis reactions, yields of (d) steam and (e) methanol, and (f) rate of methanol dehydration along the reaction channel at different syngas feed pressures.

actions 2.1 and 2.2, both of which release heat that favors the reactions also kinetically. Higher temperatures, however, are also accompanied by their faster decrease along the

channel length due to thermodynamic limitations that become more significant with temperature. The resulting trade-off between pressure and temperature also explains the gap between successive temperature profiles which become closer at higher pressures (Figure 4.3a). A similar trend is observed in the CO conversions that increase from 17% to 49% upon 40 bar increase in the inlet pressure, with its contribution becoming monotonically lesser at its higher values (Figure 4.3b). The impact of feed pressure on the rates of synthesis reactions are presented in Figure 4.3c. Regardless of the route, rates are doubled at the channel entrance upon imposing 40 bar increase in the feed pressure. Nevertheless, this promotion diminishes along the channel due to the stronger thermodynamic opposition driven by pressure-induced exothermic heat release.

In contrast with Reaction 2.1, the reverse of CO₂ hydrogenation is found to become more effective at lower pressures in a bigger portion of the channel volume as evident by the comparison of the negativity of the rates of Reaction 2.2. This trend explains the spatial evolution of in-situ steam production which is favored at higher pressures (Figure 4.3d). After reaching peak yields between 1.1–3.5%, steam is consumed by the reversal of Reaction 2.2. The locus of peak points consistently shifts to the upstream of the channel due to the earlier shift in the Reaction 2.2 at reduced pressures (Figures 4.3c and 4.3d). Yields of methanol, on the other hand, follow trends parallel to those of CO conversion, a strong indication of the dominance of CO hydrogenation on methanol synthesis (Figure 4.3e). This finding is aligned with its rates consistently above those of CO₂ hydrogenation (Figure 4.3c). Nevertheless, Reaction 2.2 has some contribution to methanol production, whose extent increases at higher pressures where the gaps between successive methanol yield curves are wider than those of conversion profiles. This contribution, however, remains below that caused by the changing the inlet temperature. Figure 4.3f gives the rate of Reaction 2.3 as a function of channel length. As more methanol is synthesized from Reactions 2.1 and 2.2 at elevated pressures, methanol dehydration is ultimately favored, notable by its acceleration at the inlet, and gives DME yields increasing from 2.2 to 3.3% (Table 4.1).

Considering the disadvantages of steam for the DME synthesis, feeding syngas at 20 bar seems favorable as it ends up with the lowest steam yield among other pressures (Figure 4.3d). However, the significantly higher CO conversions, methanol and DME yields make 50 bar a meaningful choice. Owing to the high costs of compression and incremental differences between 50 and 60 bars, the former seems to be feasible also in terms of reactor performance per unit operating cost.

4.4. Effect of Molar Inlet H₂/CO ratio

The effect of molar inlet H₂/CO on the spatial evolution of the reaction channel temperature, reaction rates, CO conversion and yields of methanol and steam are presented in Figure 4.4. Ratios of 2.5, 3.5 and 4 are studied by keeping the molar feed flow rate of H₂ constant, but changing that of CO. While doing so, total syngas flow rate is kept constant by adjusting the flow of inert N₂ accordingly. As explained in Sections 4.2 and 4.3, temperature distribution involves the common trend of a sharp rise at the very inlet, followed by a decrease along the remainder of the channel. Considering that the coolant feed properties are constant in each case, lower H₂/CO ratios lead to higher and faster declining temperatures (Figure 4.4a).

This finding is somewhat linked with the input of more N₂ to keep the total inlet flow rate constant at higher H₂/CO values, i.e. reduced CO feed flow rates which artificially lead to higher CO conversions (Figure 4.4b) due to its definition provided in Section 3.3. However, molar flow rates of converted CO follow the decreasing order of $8.04 \times 10^{-8} > 7.18 \times 10^{-8} > 6.48 \times 10^{-8}$ mol s⁻¹ at ratios of 2.5, 3.5 and 4, respectively, which is in alignment with the corresponding temperature profiles. Analysis of the rates of Reactions 2.1 and 2.2, presented in Figure 4.4c, provides further insight into understanding the implications of feed ratio. It is obvious that both reactions turn out to have higher rates at H₂/CO=2.5. The only exception to this trend is at the channel upstream where CO-lean feeding offers better promotion of the reactions, which, however, does not affect the temperatures and CO conversions mentioned above. Regardless of the feed composition, rates of both reactions approach to zero. In other words, neither of the reactions produce heat, leading to the equalization of the effluent

temperature with that of the coolant inlet of 508 K (Figure 4.4a).

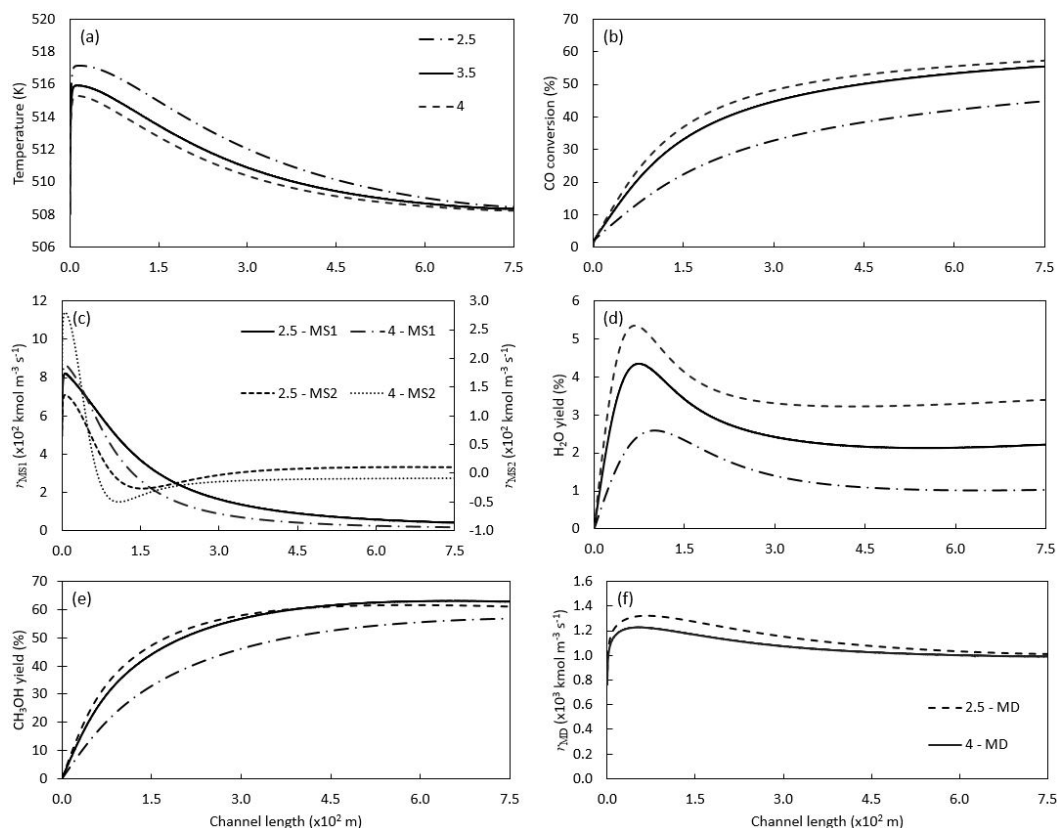


Figure 4.4. Evolution of (a) temperature, (b) CO conversion, (c) rates of methanol synthesis reactions, yields of (d) steam and (e) methanol, and (f) rate of methanol dehydration along the reaction channel at different molar inlet H₂/CO ratios

Yields of steam and methanol are presented in Figures 4.4d and 4.4e, respectively. Qualitative evolution of steam yield is dictated by the rate of CO₂ hydrogenation, whose local increase at the channel upstream leads to peaking of steam production. Due to the use of CO feed flow rate in the yield definitions, however, it is better to compare the molar flow rates of steam and methanol at the reactor exit. The amount of effluent steam is calculated as 2.06×10^{-9} , 3.08×10^{-9} and 4.05×10^{-9} mol s⁻¹ at H₂/CO of 2.5, 3.5 and 4, respectively, and follows the same qualitative response of per cent yield against feed ratio reported in Figure 4.4d. These findings justify the existence of RWGS (Reaction 2.4) as the reaction becomes favored under CO-lean conditions to produce steam. Note that RWGS is considered in the simulations as it is a function of Reactions 2.1 and 2.2. On the other hand, amounts of effluent methanol change as

1.05×10^{-7} , 8.45×10^{-8} and 7.24×10^{-8} mol s⁻¹ upon increasing H₂/CO as 2.5, 3.5 and 4, respectively. This trend is the opposite of what is reported in Figure 4.4e. Contribution of Reaction 2.2 to methanol synthesis can be quantified by subtracting the amount of CO converted, which is also equal to methanol produced by Reaction 2.1, from the total methanol amount at the exit. The resulting differences, 2.1×10^{-8} , 1.27×10^{-8} , 7.6×10^{-9} mol s⁻¹ at H₂/CO=2.5, 3.5 and 4, respectively are in perfect agreement with the decreasing order of the respective rates of Reaction 2.2 presented in Figure 4.4c.

The amounts and rates of DME synthesis as functions of H₂/CO ratio are reported in Table 4.1 and Figure 4.4f, respectively. Since its rate is one order of magnitude lower than those of synthesis reactions, the exotherm generated by Reaction 2.3 has negligible impact on the reaction temperature, which, as explained above, follows the rate patterns of Reactions 2.1 and 2.2. In alignment with the amount of methanol produced, DME synthesis is favored at the lowest feed ratio of 2.5 and found as 8.42×10^{-9} mol s⁻¹, which is 10% above the DME throughput of 7.64×10^{-9} mol s⁻¹ obtained at H₂/CO=4. The present findings show that molar inlet H₂/CO ratio of 2.5 offers the best performance in terms of increased DME production and suppressed steam formation.

4.5. Effect of molar inlet H₂/CO₂ ratio

The effect of molar inlet H₂/CO₂ on the spatial evolution of the reaction channel temperature, reaction rates, CO conversion and yields of methanol and steam are presented in Figure 4.5. Ratios of 5, 7.5, 10 and 12 are studied by keeping the molar feed flow rate of H₂ constant, but changing that of CO₂ in the context of the strategy explained in Section 4.4. The results indicate a clear pattern involving higher peak temperatures, accompanied by their faster spatial decline and elevated CO conversions as the feed gets leaner with CO₂. Moreover, the magnitude of CO₂ feeding is notable at H₂/CO₂ between 5 and 10, but remains negligible at values above 10 (Figures 4.5a and 4.5b). The root cause of this finding is associated with the presence of CO₂ as a reactant in Reaction 2.2. As H₂/CO₂ gets lower upon abundant CO₂ feeding, the extent of CO₂ hydrogenation increases to boost methanol formation, which, however

suppresses Reaction 2.1. This argument is quantified by plotting the rates of synthesis reactions at the extreme ratios of 5 and 12 along the reaction channel in Figure 4.5c. In fact, the difference in favor of the rate of Reaction 2.1 at $H_2/CO_2=12$ is obvious especially at the channel upstream. Since the channel temperature is dictated mostly by the heat release from Reaction 2.1, its promotion leads to the highest peak temperature close to 518 K (Figure 4.5a) driving Reaction 2.2 up to a maximum rate of 1.5×10^{-2} $kmol\ m^{-3}\ s^{-1}$ immediately at the inlet. Suppression of Reaction 2.1, on the other

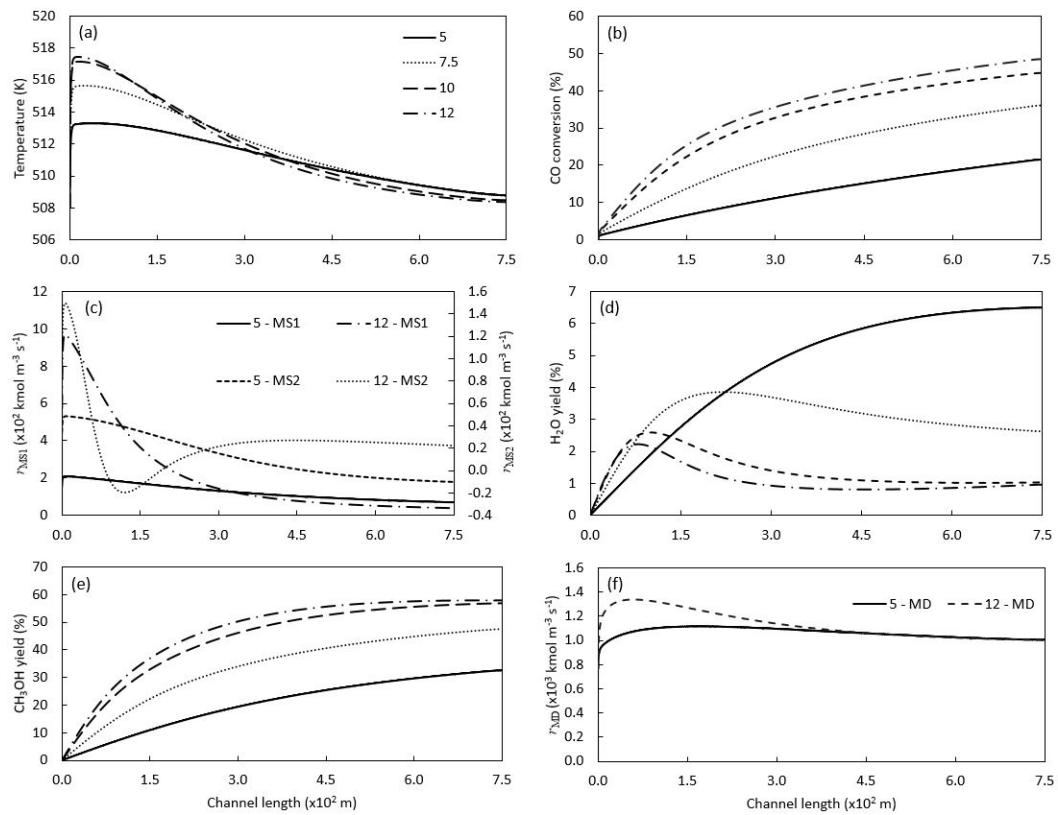


Figure 4.5. Evolution of (a) temperature, (b) CO conversion, (c) rates of methanol synthesis reactions, yields of (d) steam and (e) methanol, and (f) rate of methanol dehydration along the reaction channel at different molar inlet H_2/CO_2 ratios

hand, at $H_2/CO_2=5$ is evident from its rate that is 5 times less than obtained at the ratio of 12 (channel inlet, Figure 4.5c), causing T-rise limited by only 5 K. Despite this effect, rate of CO_2 hydrogenation remains positive in the first half of the channel due to increased dosing of CO_2 that pushes the reaction in the forward direction and elevates H_2O yields as presented in Figure 4.5d. At maximum CO_2 feeding, H_2O yield

exceeds 6% which is at least two times above those obtained at higher H_2/CO_2 ratios. Moreover, in contrast with other cases, evolution of steam formation at $H_2/CO_2=5$ do not decrease and clearly follows the path of Reaction 2.2.

Comparison of methanol yields (Figure 4.5e) with CO conversions provides insight into the change in the extent of contribution of CO_2 hydrogenation to methanol synthesis. The results justify the suppression of methanol formation as the feed becomes richer with CO_2 . For example, at channel length of 1.5×10^{-2} m, increase in methanol yield due to Reaction 2.2 is calculated as 43% and 52% at H_2/CO_2 of 5 and 12, respectively. This decrease together with lower temperatures and elevated steam yields are reflected as reduced methanol dehydration rates as shown in Figure 4.5f. Reducing inlet CO_2 elevates the DME formation rates in the first half of the channel, leading to up to 16% increase in DME yields (Table 4.1). These findings indicate that the desired reactor performance is possible at minimum dosing of CO_2 . Owing to the negligible gap between the responses obtained at ratios 10 and 12, it might be meaningful to set H_2/CO_2 ratio to 10, equivalent to 4.1% (by volume) of CO_2 in the feed, for the sake of valorizing more CO_2 , as also pointed out in the literature [9, 42]. This conclusion, however, does not imply the complete removal of CO_2 from the syngas mixture. Considering the fact that syngas mixtures can include steam from the hydrocarbon-to-syngas conversion routes [7, 76], methanol produced by Reaction 2.1 can be consumed by H_2O via the reverse of Reaction 2.2 in the absence of CO_2 at the inlet. In such cases, feeding some CO_2 may hinder the undesired conversion of methanol needed for DME synthesis. Finally, strategies for in-situ removal of H_2O from the reaction medium, such as sorption enhanced DME synthesis, can widen the window of CO_2 feeding and allow increased valorization of CO_2 , which is highly desirable from an environmental point of view [77, 78].

4.6. Effects of Inlet Flow Rate

Inlet linear flow rate of syngas is studied as another operating parameter in the range of $1-3 \times 10^{-1}$ m s^{-1} . The change in velocity is realized by increasing the molar flow rates of the reactants accordingly at the default composition, temperature and pressure

specified in Section 3.3. Increasing linear velocity from 1 to $2 \times 10^{-1} \text{ m s}^{-1}$ elevates the hot-spot from 517 to 523 K, while the further increase from 2 to $3 \times 10^{-1} \text{ m s}^{-1}$ leads to formation of 528 K as the peak temperature (Figure 4.6a).

Considering that the inlet coolant linear flow rate is kept constant at 10 m s^{-1} in three of the cases, contact of increased quantities of CO also elevates its converted amount, and the subsequent exothermic heat release that eventually escalates the temperatures. As mentioned in Sections 4.3 and 4.5, temperature distribution is mostly dictated by Reaction 2.1 due to its rate and enthalpy both of which are consistently above those of Reactions 2.2 and 2.3. Indeed, amount of CO converted is computed as 8.04×10^{-8} , 1.29×10^{-7} and $1.70 \times 10^{-7} \text{ mol s}^{-1}$ at inlet velocities of 1, 2 and $3 \times 10^{-1} \text{ m s}^{-1}$, respectively. This finding clearly justifies the link between temperature and extent of

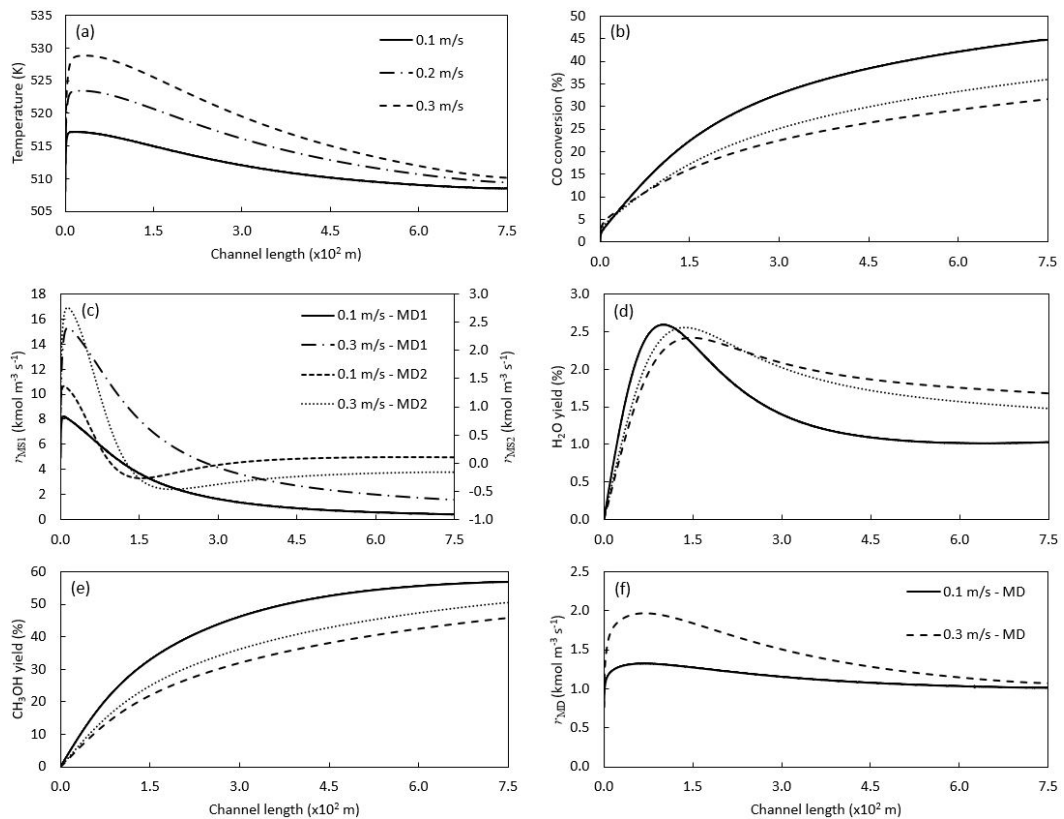


Figure 4.6. Evolution of (a) temperature, (b) CO conversion, (c) rates of methanol synthesis reactions, yields of (d) steam and (e) methanol, and (f) rate of methanol dehydration along the reaction channel at different molar inlet velocities.

CO hydrogenation. However, increased velocities reduce the duration of contact of the reactive flow with the catalyst, and somewhat suppresses the impact aforementioned outcomes. For example, the increase in the amount of CO converted is 4.86×10^{-8} and 4.1×10^{-8} mol s⁻¹ when the velocity is changed from 1 to 2×10^{-1} m s⁻¹ and from 2 to 3×10^{-1} m s⁻¹, respectively. The same effect also leads to slight decreases in the changes in the produced amounts of methanol (from 8.3×10^{-8} to 6.8×10^{-8} mol s⁻¹) and DME (from 2.9×10^{-9} to 2.8×10^{-9} mol s⁻¹). Reduced contact time also leads to a progressive shift in the locus of the hot-spots towards the downstream of the channel (Figure 4.6a). Higher feed velocities favor CO conversion and DME production at the expense of 4 times increase in the molar flow rate of effluent steam. When this is combined with the higher temperatures, the risk of hydrothermal sintering of the catalysts inherently increase. In this respect, operation at the lowest velocity of 1×10^{-1} m s⁻¹ remains to offer a safe operation with minimized risk of catalyst deactivation.

4.7. Effects of Wall Thickness and Material

Effects of thickness of the solid wall between the channels and material of construction on the investigated parameters are presented in Figures 4.7 and 4.8, respectively. Temperature profiles throughout the channel are found to increase by increasing thickness from 1 to 2×10^{-3} m (Figure 4.7a). The reason for this behavior is decreased rate of heat flux as the solid wall gets thicker. This qualitative trends, however, has minor quantitative implications on temperature profiles that differ only by <2 K leading to differences of 0.2% and 0.4% in DME yield and CO conversion, respectively. Reaction 2.2 seems to be more sensitive to temperature changes compared to Reaction 2.1 and Reaction 2.3 as only differing reaction rate is observed in the former, whereas the latter two stay almost the same when thickness of the solid wall is doubled. Relatively higher temperature distribution leads Reaction 2.2 to be reversed, which leads to more CO₂ in the reaction system and results in more H₂O yield at the outlet of the reactor due to RWGS reaction. Reversed Reaction 2.2 also causes lower methanol yield since methanol is one the products of it.

The same pattern is valid in the simulation of reactors constructed of different materials, namely cordierite and FeCrAl, in addition to stainless steel, the default material, having thermal conductivities of 3, 14.2 and 15 W m⁻¹ K⁻¹, respectively. The results indicate that hot-spot formation is qualitatively dampened, i.e. the effect

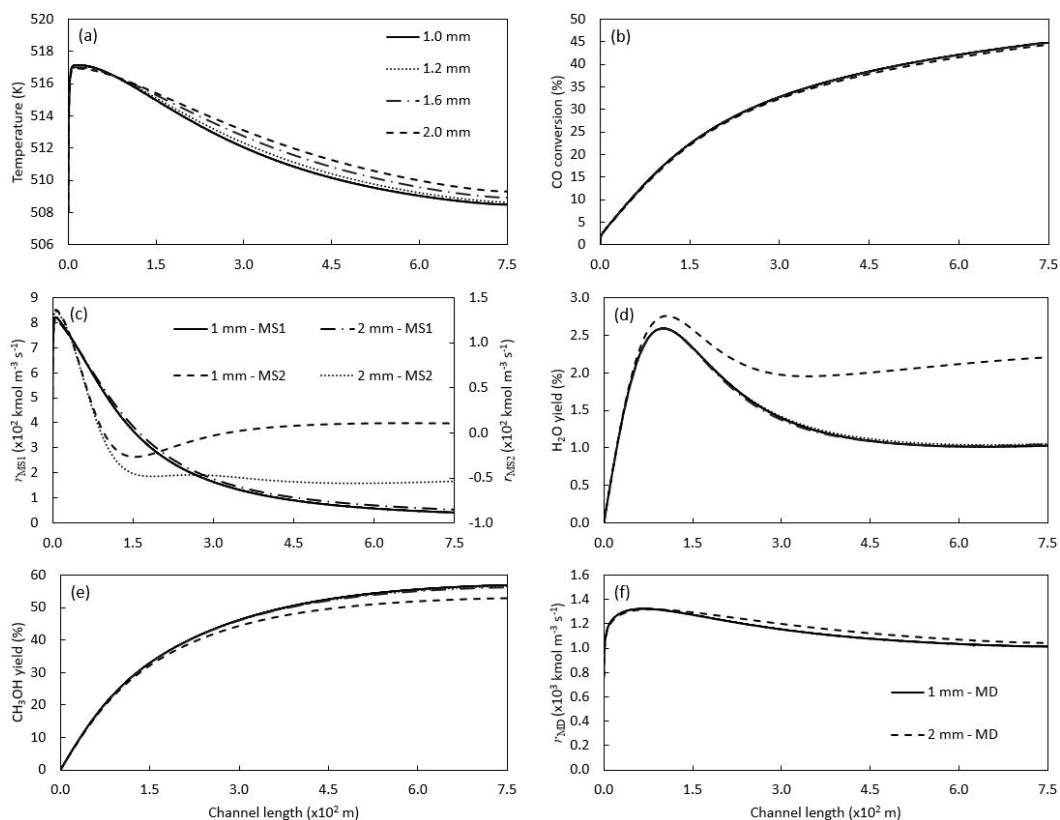


Figure 4.7. Evolution of (a) temperature, (b) CO conversion, (c) rates of methanol synthesis reactions, yields of (d) steam and (e) methanol, and (f) rate of methanol dehydration along the reaction channel at different solid wall thickness values.

of cooling is better distributed by the promotion of the axial component of the heat flux upon using thicker walls with higher thermal conductivities. This argument is commonly observed in the heat-exchange integrated microchannel reactors used to run other exothermic [64, 65, 71] and endothermic [69] reactions, and provides insight into microreactor construction strategies allowing further regulation of reaction temperature via integrated heat transfer. Similar to wall thickness, Reaction 2.2 is affected the most to temperature change, which in the end decreases methanol yield and increase H₂O yield.

Considering the operating conditions of the present work, however, the choice of wall thickness and material will be dictated by the overall volume of the multichannel reactor block, as well as method and cost of reactor construction. In the light of these findings, stainless steel is suitable material for the proposed reactor due to its ease of application, excellent mechanical properties and enhanced corrosion resistance. Thickness above 1 mm leads to a trade-off between slightly increased DME yield and CO conversion, and increased reactor construction cost. 1 mm is the optimum solid wall thickness for this work since thicker walls would increase the cost and thinner walls may cause operational problems due to high pressure values [79].

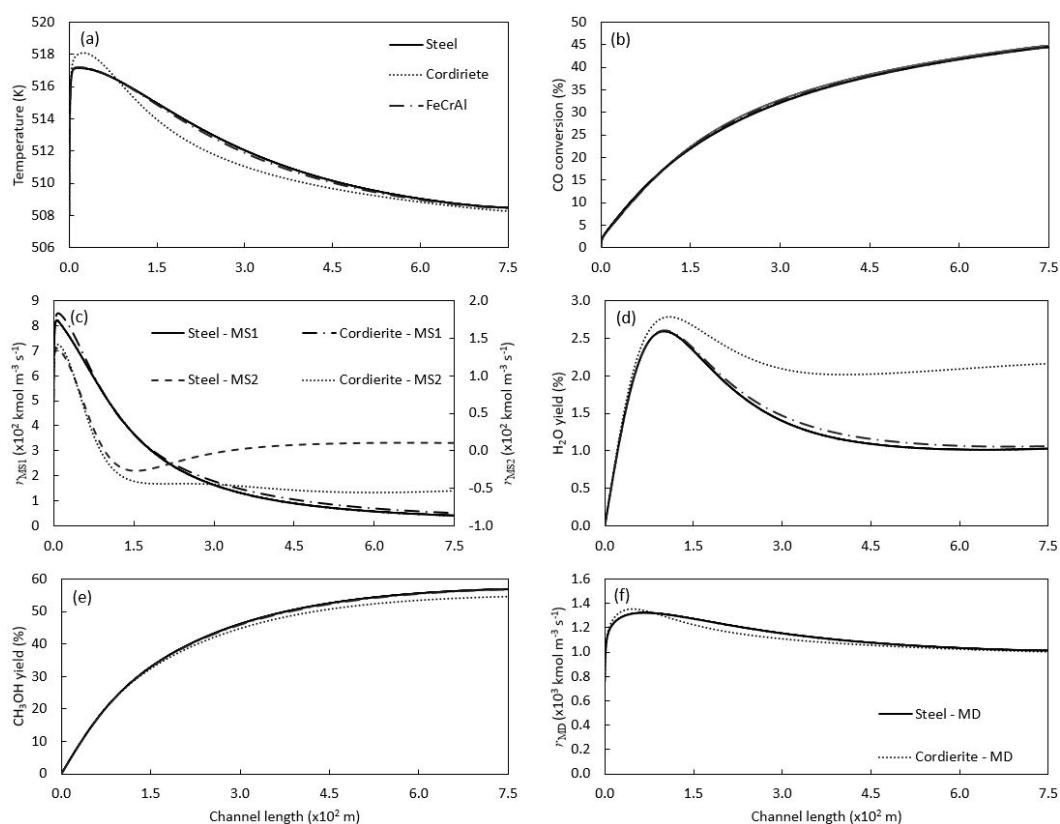


Figure 4.8. Evolution of (a) temperature, (b) CO conversion, (c) rates of methanol synthesis reactions, yields of (d) steam and (e) methanol, and (f) rate of methanol dehydration along the reaction channel at different wall materials.

4.8. Effects of Flow Partitioning

Effect of two different flow partitioning on the spatial evolution of the reaction channel temperature, reaction rates, CO conversion and yields of methanol and steam are presented in Figure 4.9. Reactive and cooling flow are fed counter-currently and co-currently to the reactor. A significant hot-spot occurs in counter-current partitioning whereas temperature is more distributed when partitioning is co-current (Figure 4.9a). The main reason for this trend is the highly exothermic reactions involved in the system. In counter-current partitioning more amount of heat can be exchange but it leads to hot-spot formation. In co-current partitioning on the other hand, hot-spot formation is prevented in the expense of less amount of heat transfer. It is also practically easier to fed the reactor with counter-current partitioning compared to co-current partitioning.

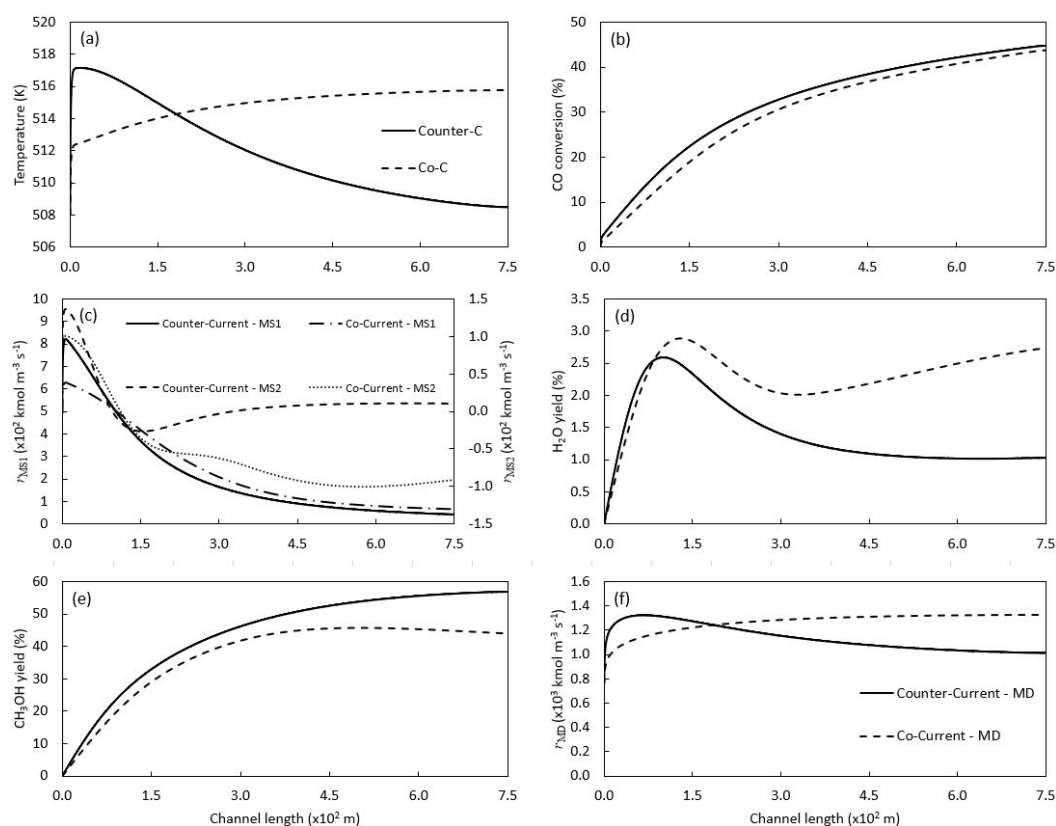


Figure 4.9. Evolution of (a) temperature, (b) CO conversion, (c) rates of methanol synthesis reactions, yields of (d) steam and (e) methanol, and (f) rate of methanol dehydration along the reaction channel at different flow partitionings.

Since kinetics of Reaction 2.2 is more sensitive than the other two, differing temperature profiles affect this parameter the most, as Reaction 2.2 stays reversed after 1.5×10^{-2} m of the reactor. This behavior decreases CO_2 conversion (Reaction 2.2), and excess CO_2 in the system forms CO and H_2O via reversed water-gas shift (Reaction 2.4). Consequently CO conversion is fewer and H_2O yield is more when the partitioning is co-current compared to those of at counter-current. Reversed Reaction 2.2 also leads to decrease in methanol yield.

Rate of Reaction 2.3 seems to be not affected with Reaction 2.1 and 2.2 since it is much slower than the other two, and shows similar behavior with temperature trends; higher the temperature higher the reaction rate. In overall rate of Reaction 2.3 is more in counter-current partitioning than that of co-current partitioning and this situation slightly enhances DME yield 3.6% to 3.9%. However, due to practical easiness, especially when larger scales of the proposed system is taken into consideration, makes counter-current partitioning the optimum selection even though it gives less DME yield.

5. CONCLUSION

DME production from syngas involving CO₂ is investigated in an air cooling integrated catalytic microchannel reactor. Hydrogenation of both CO and CO₂ to methanol and its subsequent dehydration to DME are considered to take place on Cu-ZnO/Al₂O₃ and γ -Al₂O₃, respectively, whose physical mixture at a mass ratio of 1:1 is washcoated to the inner walls of the reaction channels. The released heat is transferred to the neighboring cooling channel through a solid wall. These phenomena are simulated realistically by the two-dimensional conservation of momentum, heat and species mass together with inter-channel conductive heat exchange and reactive transport within the washcoated porous catalyst layer. After validating it by the literature-based experimental data, the model is employed to elucidate the interplay between exothermic equilibrium synthesis and dehydration reactions in the context of a detailed parametric study whose key outcomes are summarized as follows:

- Compared to its packed-bed counterparts, heat-exchange integrated microchannel reactor can suppress the magnitude of the hot spots in direct DME synthesis by $>\sim 75\%$.
- Feeding syngas and air at the same temperature offers effective regulation of hot spot formation while favoring exothermic synthesis and dehydration reactions.
- Inlet syngas temperature has the most significant impact on CO conversion and DME yield which increase from 33.1 to 44.7% and from 2 to 3.6%, respectively, upon its change from 493 to 508 K. Increase in the pressure and flow rate of syngas also favors DME production and CO consumption. While enriching the syngas with CO favors its conversion as well as DME formation, these responses are reversed upon increasing the CO₂ amount in the feed.
- Steam is an undesired intermediate that can hamper catalytic activity towards DME synthesis via sintering. In this respect, syngas feeding at 508 K, 50 bar, H₂/CO=2.5, H₂/CO₂=10 and 1×10^{-1} m s⁻¹ offers an optimal balance between minimized steam formation and increased syngas consumption together with elevated DME production.

- Thickness and material of the wall between reaction and cooling channels have negligible impacts on reactor performance. Nevertheless, use of thicker walls with high thermal conductivity characteristically offers better regulation of reaction temperature due to promotion of axial distribution of heat flux. These findings increase the number of options for determination of wall material and thickness.

5.1. Recommendations

Some recommendations for providing deeper insight into the intensification of DME synthesis and obtain higher DME yields are given below:

- Different methanol synthesis:methanol dehydration catalyst ratios other than 1:1 can be simulated to observe any possible effects of catalyst fraction. Since methanol dehydration is much slower than methanol synthesis reactions, greater ratios may enhance both CO conversion and DME yield.
- Methanol synthesis catalyst and methanol dehydration catalyst can be washcoated to opposing sides of the reactor channel.
- Instead of using a physical mixture of catalysts both of them can be washcoated sequentially one after another.
- Hot-spot formation can be dampened by allowing faster cooling flow which would enhance the axial distribution of heat flux along the reactor.
- Cooling flow can be fed at a temperature higher than syngas flow since the former is more dominant than the latter regarding overall reactor temperature profile.
- Pressure of the cooling flow can be decreased regarding cost issues.

REFERENCES

1. Martins, J. M., F. Guo and D. A. Swanson, “Chapter 1 - Population: Survival and Growth”, *Global Population in Transition*, pp. 1–41, Springer, Cham, 2018.
2. Cheng, J., *Biomass to Renewable Energy Processes*, CRC Press, 2017.
3. Ellabban, O., H. Abu-Rub and F. Blaabjerg, “Renewable energy resources: Current status, future prospects and their enabling technology”, *Renewable and Sustainable Energy Reviews*, Vol. 39, pp. 748–764, 2014.
4. Azizi, Z., M. Rezaeimanes, T. Tohidian and M. R. Rahimpour, “Dimethyl Ether: A review of Technologies and Production Challenges”, *Chemical Engineering and Processing: Process Intensification*, Vol. 82, pp. 150–172, 2014.
5. Huang, M.-H., H.-M. Lee, K.-C. Liang, C.-C. Tzeng and W.-H. Chen, “An experimental study on single-step dimethyl ether (DME) synthesis from hydrogen and carbon monoxide under various catalyst”, *International Journal of Hydrogen Energy*, pp. 1–11, 2015.
6. DeFalco, M., *Dimethyl Ether (DME) Production*, 2017, <http://oil-gasportal.com/dimethyl-ether-dme-production-2/>, accessed at Dec 2018.
7. Rostrup-Nielsen, J., “New Aspects of Syngas Production and Use”, *Catalysis Today*, Vol. 63, pp. 159–164, 2000.
8. Saravanan, K., H. Ham, N. Tsubaki and J. W. Bae, “Recent Progress for Direct Synthesis of Dimethyl Ether from Syngas on the Heterogeneous Bifunctional Hybrid Catalysts”, *Applied Catalysis B: Environmental*, Vol. 217, pp. 494–522, 2017.
9. Peláez, R., P. Marín and S. Ordóñez, “Direct synthesis of dimethyl ether from

- syngas over mechanical mixtures of CuO/ZnO/Al₂O₃ and γ -Al₂O₃: Process optimization and kinetic modelling”, *Fuel Processing Technology*, Vol. 168, pp. 40–49, 2017.
10. Gadek, M., R. Kubica and E. Jedrysik, “Production of methanol and dimethyl ether from biomass derived syngas - a comparison of the different synthesis pathways by means of flowsheet simulation”, *Computer Aided Chemical Engineering*, Vol. 32, pp. 55–60, 2013.
 11. Gogate, M., “The Direct Dimethyl Ether (DME) Synthesis Process from Carbon-Based Feed Stocks: Current Status and Future Prospects II. Kinetic Studies and Catalyst Deactivation”, *Progress in Petrochemical Science*, Vol. 2, 2018.
 12. Fleisch, T. H., A. Basu and R. A. Sills, “Introduction and Advancement of a New Clean Global Fuel: The Status of DME Developments in China and Beyond”, *Journal of Natural Gas Science and Engineering*, Vol. 9, pp. 94–107, 2012.
 13. Chen, W. H. and X. D. Wang, “Thermodynamic approach and comparison of two- step and single step DME (dimethyl ether) syntheses with carbon dioxide utilization”, *Energy*, Vol. 109, pp. 326–340, 2016.
 14. Vakili, R., E. Pourazadi, P. Setoodeh, R. Eslamloueyan and M. R. Rahimpour, “Direct dimethyl ether (DME) synthesis through a thermally coupled heat exchanger reactor”, *Applied Energy*, Vol. 88, pp. 1211–1223, 2011.
 15. Hu, Y., Z. Nie and D. Fang, “Simulation and model design of pipe-shell reactor for the direct synthesis of dimethyl ether from syngas”, *Journal of Natural Gas Chemistry*, Vol. 17, pp. 195–200, 2008.
 16. Venvik, H. J. and J. Yang, “Catalysis in microstructured reactors: Short review on small-scale syngas production and further conversion into methanol, DME and Fischer-Tropsch products”, *Catalysis Today*, Vol. 285, pp. 135–146, 2017.

17. Aguayo, A. T., J. Erena, D. Mier, J. M. Arandes, M. Olazar and J. Bilbao, "Kinetic Modeling of Dimethyl Ether Synthesis in a Single Step on a CuO–ZnO–Al₂O₃/γ–Al₂O₃ catalyst", *Industrial Engineering Chemistry Research*, Vol. 46, pp. 5522–5530, 2007.
18. Hosseinienejad, S., A. Afacan and R. Hayes, "Catalytic and kinetic study of methanol dehydration to dimethyl ether", *Chemical Engineering Research and Design*, Vol. 90, pp. 825–833, 2012.
19. Volkov, V., E. Novitskii, G. Dibrov, P. Samokhin, M. Kipnis and A. Yaroslavtsev, "Modeling, simulation and control of dimethyl ether synthesis in an industrial fixed-bed reactor", *Chemical Engineering and Processing: Process Intensification*, Vol. 50, pp. 85–94, 2011.
20. Liua, Y., S. Podila, D. Nguyen, D. E. P. Nguyen, C. Pham, M. Ledoux and C. Pham-Huu, "Methanol dehydration to dimethyl ether in a platelet milli-reactor filled with H-ZSM5/SiC foam catalyst", *Applied Catalysis A: General*, Vol. 409–410, pp. 113–121, 2011.
21. Mao, D., W. Yang, J. Xia, B. Zhang and G. Lu, "The direct synthesis of dimethyl ether from syngas over hybrid catalysts with sulfate-modified γ-alumina as methanol dehydration components", *Journal of Molecular Catalysis A: Chemical*, Vol. 250, pp. 138–144, 2006.
22. Raoof, F., M. Taghizadeh, A. Eliassi and F. Yaripour, "Effects of temperature and feed composition on catalytic dehydration of methanol to dimethyl ether over γ-alumina", *Fuel*, Vol. 87, pp. 2967–2971, 2008.
23. Yaripour, F., F. Baghaei, I. Schmidt and J. Perregaard, "Catalytic dehydration of methanol to dimethyl ether over solid acid catalysts", *Catalysis Communications*, Vol. 6, p. 147, 2005.
24. Xu, M., J. Lunsford and D. Goodman, "Synthesis of dimethyl ether (DME) from

- methanol over solid-acid catalysts”, *Applied Catalysis A: General*, Vol. 149, pp. 289–301, 1997.
25. Ramos, F., A. Duarte de Farias, L. Borges, J. Monteiro, M. Fraga, E. Sousa-Aguiar and L. Appel, “Role of dehydration catalyst acid properties on one-step DME synthesis over physical mixtures”, *Catalysis Today*, Vol. 101, pp. 39–44, 2005.
 26. Fei, J., Z. Hou, B. Zhu, H. Lou and X. Zheng, “Synthesis of dimethyl ether (DME) on modified HY zeolite and modified HY zeolite-supported Cu–Mn–Zn catalysts”, *Applied Catalysis A: General*, Vol. 304, pp. 49–54, 2006.
 27. Moradi, G., F. Yaripour and P. Vale-Sheyda, “Catalytic dehydration of methanol to dimethyl ether over mordenite catalysts”, *Fuel Process. Technology*, Vol. 91, pp. 461–468, 2009.
 28. Tokay, K., T. Doğu and G. Doğu, “Dimethyl ether synthesis over alumina based catalysts”, *Chemical Engineering Journal*, Vol. 184, pp. 278–285, 2012.
 29. Jiang, S., Y. Hwang, S. Jhung, J. Chang, J. Hwang, T. Cai and S. Park, “Zeolite SUZ-4 as selective dehydration catalyst for methanol conversion to dimethyl ether”, *Chemistry Letters*, Vol. 33, pp. 1048–1049, 2004.
 30. Gates, B. and L. Johanson, “Dehydration of the alcohol in the etherification of isoamylenes with methanol and ethanol”, *Industrial Engineering Chemistry Research*, Vol. 17, pp. 981–983, 1971.
 31. Kiviranta-Paakkönen, P., L. Struckmann, J. Linnekoski and A. Krause, “Langmuir-Hinshelwood kinetics of the dehydration of methanol catalyzed by cation exchange resin”, *Industrial Engineering Chemistry Research*, Vol. 37, pp. 18–24, 1998.
 32. Liwei, Z., W. Junhua, W. Pei, H. Zhaoyin, F. Jinhua and Z. Xiaoming, “Synthesis of Dimethyl Ether via Methanol Dehydration over Combined Al₂O₃-HZSM-5 Solid Acids”, *Chinese Journal of Catalysis*, Vol. 31, pp. 987–992, 2010.

33. Zhu, Y., S. Wang, X. Ge, Q. Liu, Z. Luo and K. Cen, “Experimental study of improved two step synthesis for DME production”, *Fuel Processing Technology*, Vol. 91, pp. 424–429, 2010.
34. Erena, J., I. Sierra, M. Olazar, A. G. Gayubo and A. T. Aguayo, “Deactivation of a CuO–ZnO–Al₂O₃/γ–Al₂O₃ catalyst in the synthesis of dimethyl ether”, *Industrial Engineering Chemistry Research*, Vol. 47, pp. 2238–2247, 2008.
35. Kang, S. H., J. W. Bae, H. S. Kim, G. M. Dhar and K. W. Jun, “Enhanced catalytic performance for dimethyl ether synthesis from syngas with the addition of Zr or Ga on a Cu–ZnO–Al₂O₃/γ–Al₂O₃ bifunctional catalyst”, *Energy Fuels*, Vol. 24, pp. 804–810, 2010.
36. Wang, Y., W. Wang, Y. Chen, J. Mar and R. Li, “Synthesis of dimethyl ether from syngas over core–shell structure catalyst CuO–ZnO–Al₂O₃@SiO₂–Al₂O₃”, *Chemical Engineering Journal*, Vol. 250, pp. 248–256, 2014.
37. Phienluphon, R., K. Pinkaew, G. Yang, J. Li, Q. Wei, Y. Yoneyama, T. Vitidsant and N. Tsubaki, “Designing core (Cu/ZnO/Al₂O₃)–shell (SAPO-11) zeolite capsule catalyst with a facile physical way for dimethyl ether direct synthesis from syngas”, *Chemical Engineering Journal*, Vol. 270, pp. 605–611, 2015.
38. Lee, Y. J., M. H. Jung, J. B. Lee, K. E. Jeong, H. S. Roh, Y. W. Suh and J. W. Bae, “Single-step synthesis of dimethyl ether from syngas on Al₂O₃-modified CuO–ZnO–Al₂O₃/ferrierite catalysts: Effects of Al₂O₃ content”, *Catalysis Today*, Vol. 228, pp. 175–182, 2014.
39. Montesano, R., A. Narvaez and D. Chadwick, “Shape-selectivity effects in syngas-to-dimethyl ether conversion over Cu/ZnO/Al₂O₃ and zeolite mixtures: Carbon deposition and by-product formation”, *Applied Catalysis A: General*, Vol. 482, pp. 69–77, 2014.
40. Cai, M., V. Subramanian, V. V. Sushkevich, V. V. Ordonsky and A. Y. Khodakov,

- “Effect of Sn additives on the CuZnAl–HZSM-5 hybrid catalysts for the direct DME synthesis from syngas”, *Applied Catalysis A: General*, Vol. 502, pp. 370–379, 2015.
41. Xie, Q., P. Chen, P. Peng, S. Liu, P. Peng, B. Zhang, Y. Cheng, Y. Wan, Y. Liu and R. Ruan, “Single-step synthesis of DME from syngas on CuZnAl–zeolite bifunctional catalysts: the influence of zeolite type”, *RSC Advances*, Vol. 5, pp. 26301–26307, 2015.
42. Erena, J., I. Sierra, A. T. Aguayo, A. Ateka, M. Olazar and J. Bilbao, “Kinetic modelling of dimethyl ether synthesis from (H_2+CO_2) by considering catalyst deactivation”, *Chemical Engineering Journal*, Vol. 174, pp. 660–667, 2011.
43. Naik, S. P., T. Ryu, V. Bui, J. D. Miller, N. B. Drinnan and W. Zmierzak, “Synthesis of DME from CO_2/H_2 gas mixture”, *Chemical Engineering Journal*, Vol. 167, pp. 362–368, 2011.
44. Zhang, Y., D. Li, S. Zhang, K. Wang and J. Wu, “ CO_2 hydrogenation to dimethyl ether over CuO–ZnO– Al_2O_3 /HZSM-5 prepared by combustion route”, *RSC Advances*, Vol. 4, pp. 16391–16396, 2014.
45. Zhao, Y., J. Chen and J. Zhang, “Effects of ZrO_2 on the performance of CuO–ZnO– Al_2O_3 /HZSM-5 catalyst for dimethyl ether synthesis from CO_2 hydrogenation”, *Journal of Natural Gas Chemistry*, Vol. 16, pp. 382–392, 2007.
46. Sun, J. T., I. S. Metcalfe and M. Sahibzada, “Deactivation of Cu/ZnO/ Al_2O_3 methanol synthesis catalyst by sintering”, *Industrial Engineering Chemistry Research*, Vol. 38, pp. 3868–3872, 1999.
47. Hu, J., Y. W. C. Cao, D. C. Elliott, D. J. Stevens and J. F. White, “Conversion of biomass syngas to DME using a microchannel reactor”, *Industrial Engineering Chemistry Research*, Vol. 44, pp. 1722–1727, 2005.
48. Hayer, F., H. Bakhtiary-Davijany, R. Myrstad, A. Holmen, P. Pfeifer and H. J.

- Venkov, "Modeling and simulation of an integrated micro packed bed reactor-heat exchanger configuration for direct dimethyl ether synthesis", *Topics in Catalysis*, Vol. 54, p. 817, 2011.
49. Hayer, F., H. Bakhtiary-Davijany, R. Myrstad, A. Holmen, P. Pfeifer and H. J. Venkov, "Synthesis of dimethyl ether from syngas in a microchannel reactor—Simulation and experimental study", *Chemical Engineering Journal*, Vol. 167, pp. 610–615, 2011.
50. Hayer, F., H. Bakhtiary-Davijany, R. Myrstad, A. Holmen, P. Pfeifer and H. J. Venkov, "Characteristics of integrated micro packed bed reactor-heat exchanger configurations in the direct synthesis of dimethyl ether", *Chemical Engineering and Processing: Process Intensification*, Vol. 70, pp. 77–85, 2013.
51. McBride, K., T. Turek and R. Güttel, "Direct dimethyl ether synthesis by spatial patterned catalyst arrangement: A modeling and simulation study", *AIChE Journal*, Vol. 58, pp. 2468–3473, 2012.
52. Simsek, E., A. K. Avcı and Z. I. Onsan, "Investigation of catalyst performance and microstructured reactor configuration for syngas production by methane steam reforming", *Catalysis Today*, Vol. 178, pp. 157–163, 2011.
53. Simsek, E., A. K. Avcı and Z. I. Onsan, "Oxidative steam reforming of methane to synthesis gas in microchannel reactors", *International Journal of Hydrogen Energy*, Vol. 38, pp. 870–878, 2013.
54. Kolb, G. and V. Hessel, "Micro-structured reactors for gas phase reactions", *Chemical Engineering Journal*, Vol. 98, pp. 1–38, 2004.
55. Kiwi-Minsker, L. and A. Renken, "Microstructured reactors for catalytic reactions", *Catalysis Today*, Vol. 110, pp. 2–14, 2005.
56. Delparish, A. and A. K. Avcı, "Intensified catalytic reactors for Fischer-Tropsch

- synthesis and for reforming of renewable fuels to hydrogen and synthesis gas”, *Fuel Processing Technology*, Vol. 151, pp. 72–100, 2016.
57. Onsan, Z. I. and A. K. Avci, *Multiphase Catalytic Reactors: Theory, Design, Manufacturing, and Applications*, Wiley, Hoboken, 2016.
 58. Kolb, G., “Review: Microstructured reactors for distributed and renewable production of fuels and electrical energy”, *Chemical Engineering and Processing*, Vol. 65, pp. 1–44, 2013.
 59. Onsan, Z. I. and A. K. Avci, “Chapter 14 - Reactor Design for Fuel Processing”, D. Shekhawat, J. J. Spivey and D. A. Berry (Editors), *Fuel Cells: Technologies for Fuel Processing*, pp. 451–516, Elsevier Science, Amsterdam, 2011.
 60. Rebrov, E. V., M. H. J. M. de Croon and J. C. Schouten, “Design of a microstructured reactor with integrated heat-exchanger for optimum performance of a highly exothermic reaction”, *Catalysis Today*, Vol. 69, pp. 183–192, 2001.
 61. Rebrov, E. V., M. H. J. M. de Croon and J. C. Schouten, “Development of the kinetic model of platinum catalyzed ammonia oxidation in a microreactor”, *Chemical Engineering Journal*, Vol. 90, pp. 61–76, 2002.
 62. Ehrfeld, W., V. Hessel and H. Löwe, *Microreactors: New Technology for Modern Chemistry*, Wiley WCH, Weinheim, 2016.
 63. Uriz, I., G. Arzamendi, E. López, J. Llorca and L. Gandía, “Computational fluid dynamics simulation of ethanol steam reforming in catalytic wall microchannels”, *Chemical Engineering Journal*, Vol. 167, pp. 603–609, 2011.
 64. Bac, S. and A. K. Avci, “Ethylene oxide synthesis in a wall-coated microchannel reactor with integrated cooling”, *Chemical Engineering Journal*, 2018, in press.
 65. Bac, S., S. Keskin and A. K. Avci, “Modeling and simulation of water-gas shift

- in a heat exchange integrated microchannel converter”, *International Journal of Hydrogen Energy*, Vol. 43, pp. 1094–1104, 2018.
66. Karakaya, M. and A. K. Avcı, “Microchannel reactor modeling for combustion driven reforming of iso-octane”, *International Journal of Hydrogen Energy*, Vol. 36, pp. 6569–6577, 2011.
67. Goodwin, B. M., *Thermodynamic Properties of Multicomponent Systems, Multicomponent Phase Equilibria and Chemical Equilibria*, American Institute of Chemical Engineers, New York, 1982.
68. McBride, B. J., S. Gordon and M. A. Reno, *Coefficients for calculating thermodynamic and transport properties of individual species*, National Aeronautics and Space Administration, 1993.
69. Delparish, A. and A. K. Avcı, “Modeling of intensified glycerol steam reforming in a heat-exchange integrated microchannel reactor”, *Catalysis Today*, Vol. 299, pp. 328–338, 2018.
70. Portha, J. F., K. Parkhomenko, K. Kobl, A. Roger, S. Arab, J. M. Commenge and L. Falk, “Kinetics of methanol synthesis from carbon dioxide hydrogenation over copper–zinc oxide catalysts”, *Industrial Engineering Chemistry Research*, Vol. 56, pp. 13133–13145, 2017.
71. Tezcan, I. and A. K. Avcı, “Parametric investigation of oxidative coupling of methane in a heat-exchange integrated microchannel reactor”, *Journal of Chemical Technology and Biotechnology*, Vol. 90, pp. 1827–1838, 2015.
72. Karakaya, M. and A. K. Avcı, “Simulation of on-Board Fuel Conversion in Catalytic Microchannel Reactor-Heat Exchanger Systems”, *Topics in Catalysis*, Vol. 52, pp. 2112–2116, 2009.
73. Veser, G. and J. Frauhammer, “Modelling steady state and ignition during catalytic

- methane oxidation in a monolith reactor”, *Chemical Engineering Science*, Vol. 55, pp. 2271–2286, 2000.
74. Avcı, A. K., D. L. Trimm and M. Karakaya, “Microreactor catalytic combustion for chemicals processing”, *Catalysis Today*, Vol. 155, pp. 66–74, 2010.
75. Salmi, T., J. H. Carucci, M. Roche, K. Eränen, J. Wärnå and D. Murzin, “Microreactors as tools in kinetic investigations: Ethylene oxide formation on silver catalyst”, *Chemical Engineering Science*, Vol. 87, pp. 306–314, 2013.
76. Tan, O., E. Masalaci, Z. I. Onsan and A. K. Avcı, “Design of a methane processing system producing high-purity hydrogen”, *International Journal of Hydrogen Energy*, Vol. 33, pp. 5516–5526, 2008.
77. Iliuta, I., F. Larachi and P. Fongarland, “Dimethyl ether synthesis with in situ H₂O removal in fixed-bed membrane reactor: model and simulations”, *Industrial Engineering Chemistry Research*, Vol. 49, pp. 6870–6877, 2010.
78. Iliuta, I., M. C. Iliuta and F. Larachi, “Sorption-enhanced dimethyl ether synthesis—Multiscale reactor modeling”, *Chemical Engineering Science*, Vol. 66, pp. 2241–2251, 2011.
79. Jermkwan, N., P. Inbamrung, P. Narataruksa and C. Prapainainar, “Design Equations for Catalytic Microchannel Reactors: Fischer-Tropsch Synthesis”, *Energy Procedia*, Vol. 79, pp. 772–777, 2015.